CELLULAR RADIOTOXICITY OF IODINE-123

B.S. Smit

Thesis presented in partial fulfillment of the requirements for the degree of Master of Sciences (Zoology) at the University of Stellenbosch.

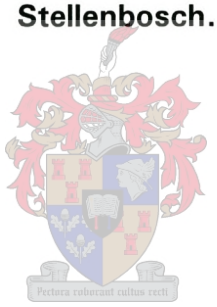

Supervisor: Prof. E.L.J.F. Böhm
Dept. of Radiation Oncology
University of Stellenbosch
Medical School
Tygerberg

Co-supervisor: Dr. S.A. Reinecke
Dept. of Zoology
University of Stellenbosch

March 2000

Declaration

I, the undersigned, hereby declare that the work contained in this thesis is my own original work and that I have not previously in its entirety or in part submitted it at any university for a degree.

ABSTRACT

The Auger electron emitter iodine-123 was examined in the form of 4-[^{123}I]iodoantipyrine and as [^{123}I]NaI for its effectiveness in killing cells of different sensitivity to photon irradiation. Micronucleus assays showed that 4-[^{123}I]iodoantipyrine is two to three times more effective in cell inactivation than [^{123}I]NaI. This can be attributed to the fact that antipyrine, for reason of its lipid solubility, can enter cells and can reach the cell nucleus, whereas [^{123}I]NaI is excluded from the cytoplasm. The differential targeting of intra- and extracellular compartments was confirmed by radionuclide uptake experiments. In the nucleus, Auger decay conceivably is located on the DNA where it may invoke high-LET irradiation damage. Irradiation damage by [^{123}I]NaI is by long range γ-irradiation and hence low-LET. Results of the present study demonstrate however that the enhancement of MN-frequency seen with 4-[^{123}I]iodoantipyrine over [^{123}I]NaI is similar for all cell lines and that the narrowing of MN-response expected for 4-[^{123}I]iodoantipyrine does not occur. Experiments with the free radical scavenger, DMSO, indicated nearly identical dose reduction factors for both iodine-123 carriers. These two observations strongly suggest that the cell inactivation by 4-[^{123}I]iodoantipyrine is not by high-LET direct ionisation of DNA, but due to an indirect effect. The indirect radiation effect of Auger decay in the nucleus is attributed to shielding of DNA by histones. Such a protection mechanism is not unrealistic if it is realised that histones and DNA associate in a 1:1 weight ratio and that higher order folding of the nucleosome chain into solenoids, loops, and chromatids generates considerable protein density. In the nucleosome core, the histone octamer measures 7 nm and closely approximates the 10 nm dimention of the Auger electron range. It is suggested that the interlacing of protein density with DNA density suppresses direct ionisation from Auger decay at the DNA and directs the majority of Auger decay to the histones.

OPSOMMING

Die Auger-elektron-uitstraler, jodium-123, is ondersoek in die vorm van 4-[^{123}I]jodoantipirien en [^{123}I]NaI om die effektiwiteit te bepaal waarmee dit selle met verskillende grade van sensitiwiteit vir fotonbestraling doodmaak. Mikrokerntellings toon aan dat 4-[^{123}I]jodoantipirien selle twee tot drie maal meer effektief inaktiveer as [^{123}I]NaI. Dit kan toegeskryf word aan die feit dat antipirien, as gevolg van sy vetoplosbaarheidseienskappe, die selle kan binnedring en die kern bereik, teenoor [^{123}I]NaI wat uitgesluit word uit die sitoplasma. Die differensiële blootstelling van intra- en ekstrasellulere gebiede is bevestig deur radionukliedopname eksperimente. In die selkern vind Auger verval waarskynlik by die DNA plaas waar dit hoë-LET stralingskade veroorsaak. Stralingskade afkomstig van [^{123}I]NaI is deur langafstand γ-strale en dus lae-LET. Die resultate van die huidige studie bewys egter dat die verhoogde mikrokernfrekwensie van 4-[^{123}I]jodoantipirien teenoor [^{123}I]NaI dieselfde is vir al die sellyne en dat die vernouïng van mikrokernreaksie soos verwag met 4-[^{123}I]jodoantipirien, nie plaasvind nie. Eksperimente met die vryradikaalopruimer, DMSO, dui op feitlik identiese dosis-modifiseringsfaktore vir beide jodium-123 draers. Hierdie twee waarnemings is 'n besliste aanduiding dat die selinaktivering deur 4-[^{123}I]jodoantipirien nie deur hoë-LET direkte ionisering van DNA plaasvind nie, maar eerder deur indirekte stralingsaksie. Die indirekte stralingseffek van Auger-verval in die kern kan toegeskryf word aan afskerming van DNA deur histone. So 'n beskermingsmeganisme is nie onrealisties nie, as in ag geneem word dat histone en DNA in 'n 1:1 gewigsverhouding assosieer en dat hoër orde vouïng van die nukleosoomketting tot solenoïede, lusse en chromatiede 'n beduidende protïendigtheid genereer. In die nukleosoomkern is die histoon-oktameer ongeveer 7 nm in deursnit en dus vergelykbaar met die 10 nm reikafstand van die Auger elektrone. Dit word voorgestel dat die ineengeweefdheid van die protien-digtheid met die DNA-digtheid die direkte ionisering van die DNA tydens Auger verval onderdruk en dat die meeste van die Auger verval in die histone plaasvind.

ACKNOWLEDGEMENTS

I would like to thank the following people:

Prof. Lothar Böhm, for his leadership as supervisor, dedicated teaching effort and valuable suggestions.

Dr. Sophié Reinecke, who gave caring advice and encouragement as co-supervisor and provided hospitality at the Zoology department.

Dr. Kobus Slabbert, for suggesting the topic, preliminary work and continued discussions to solve difficult problems.

Dr. Jan Langenhoven, for persevering in the development of a suitable iodine-123 labelled antipytrine molecule.

Stuart Dolley and Etienne Vermeulen, for the many times they have synthesized high quality 4-[^{123}I]iodoantipyrine, sometimes on very short notice.

Tony Serafin, for his generous help and advice on cell culturing.

Staff of Tygerberg and Groote Schuur Radiobiology Departments, for their suggestions, help, interest and encouragement.

NAC management, for the opportunity to execute this project at NAC and the financial contribution to my attendance of the ICRR 99.

NAC staff, for the advice, help, support and friendliness of all staff members that played a part in putting this project together.

LIST OF ABBREVIATIONS

AT - Ataxia telangiectasia

BNC - Binucleated Cell

CHO - Chinese Hamster Ovary

Ci - Curie

Cis-Pt-II - Cisplatin (*cis*-dichlorodiammineplatinum)

DMBA - Dimethyl Butyric Acid

DMSO - Dimethyl Sulphoxide

DNA - Deoxyribonucleic Acid

DRF - Dose Reduction Factor

EMEM - Eagle's Minimum Essential Medium

FCS - Fetal Calf Serum

FISH - Fluorescent In Situ Hybridization

Gy - Gray

HPLC - High Pressure Liquid Chromatography

ICRR - International Congress for Radiation Research

LET - Linear Energy Transfer

MN - Micronucleus/ei

NAC - National Accelerator Centre

OER - Oxygen Enhancement Ratio

PBS - Phosphate Buffered Saline

RBE - Relative Biological Effect

RIT - Radio-immunotherapy

rpm - revolutions per minute

RPMI - Roswell Park Memorial Institute

CONTENTS

CHAPTER 1: INTRODUCTION

1.1. General background

Auger electrons are low energy particles (~20-500 eV) with a range of 1-10 nm in tissue (Howell, 1992). Auger electrons arise from electron transitions in the inner orbitals of the atom, created by the radioactivity decay process and are found in approximately 50% of all radionuclides (Humm *et al*, 1994). Decay by electron capture or internal conversion, create a vacancy in an inner atomic shell. When an electron from the outer shells fills this vacancy, the released energy emerges as characteristic X-irradiation (photoelectric effect). In some isotope decay processes this radiation is absent and one observes monoenergetic electrons, which are ejected and which generates a second vacancy. These electrons are referred to as Auger electrons. (Fig. 1.1) (Howell 1992, Johns 1974). Auger electrons have a very short range in biological matter because of their charge and this leads to highly localized energy deposition. The linear energy transfer (LET) of Auger electrons is 10-25 keV/μm and in the same order of magnitude as alpha particles. Cobalt-60 γ-rays have a LET of 0,2 keV/μm (Hofer and Bao 1995, Hall 1988). Because of their high-LET characteristics, Auger electrons can be expected to induce pronounced cell killing.

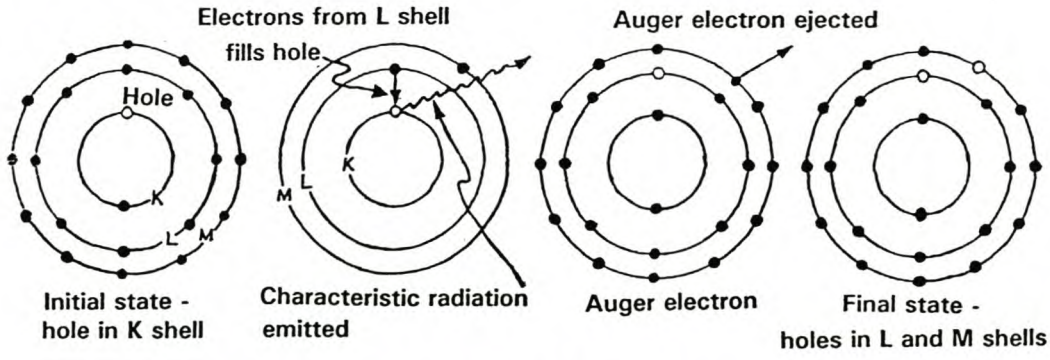

Fig. 1.1. Representation of a KLM Auger electron resulting from a hole in the K shell (Johns, 1974).

Application of Auger electron emitting radionuclides in cancer therapy holds great promise, provided selective delivery to cancer cells can be assured. Intracellular

decay of the radionuclide would restrict radiation damage to the cancer cells (Persson, 1994) and minimize damage to normal cells. High-LET irradiation is very potent because of poor repair of sublethal damage, a reduced oxygen enhancement ratio (OER) and a lower dependence upon cell phases (Hall, 1988). Auger emission in cancer cells would focus the irradiation to the tumor volume, sparing surrounding tissue. Selective radionuclide delivery to cancer cells can be accomplished using specific monoclonal antibodies labelled with the radionuclide. Radionuclide-labelled hormones, which bind to receptors in cancer cells, provide another route for selective radionuclide delivery (Kearney *et al*, 1999). A suitable radionuclide and Auger electron emitter is iodine-123, because of its ideal emission spectrum and relative short half-life, (13.2 h). Two of the eight energy levels of Auger electrons emitted by iodine-123 are responsible for 90% of the Auger electron yield per decay (Howell, 1992). The Auger electrons emitted at these two energy levels have a range of less than 20 nm and therefore induce highly localized energy deposition (Fig. 1.2).

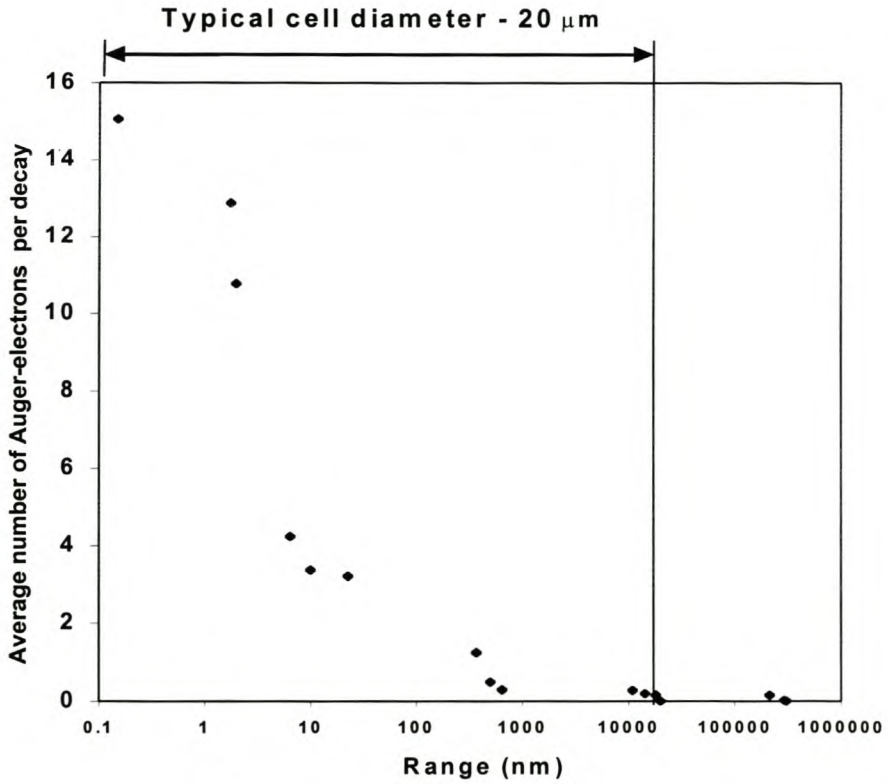

Fig. 1.2. Graph of average number of Auger electrons covering each range, calculated per decay of iodine-123.

Mammalian cells have, in comparison, typical diameters of 10-20 μm. If the energy is deposited in the cell nucleus it translates to very high radiotoxicity. These properties make iodine-123 an extremely interesting and challenging isotope for studies of cellular inactivation.

Iodine-123, produced at the National Accelerator Centre (NAC) at Faure, was used as 4-[^{123}I]iodoantipyrine and as [^{123}I]NaI. These two carriers differ with regard to uptake by the cell. Antipyrine is lipid soluble and hence will readily diffuse across the cell and nuclear membranes and would conceivably reach the cell nucleus (Fig. 1.3) (Miyazaki *et al*, 1993).

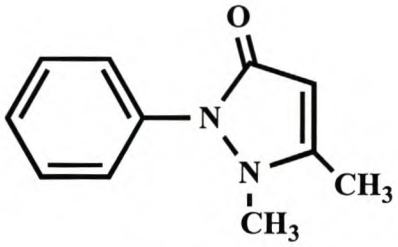

Fig. 1.3. Antipyrine (2,3-dimethyl-1-phenyl-3-pyrazolin-5-one, $C_{11}H_{12}N_2O$)

[^{123}I]NaI, on the other hand, is excluded from the cells altogether and is not accessible to the anion transport process (Kassis *et al*, 1980). The estimated pore diameter of ion channels is 0.4 to 0.8 nm. The iodine atom has a diameter of 0.264 nm, but will not easily enter these channels, because the passive permeability of ions in biological membranes is more related to the hydrated ion diameter than to the diameter of the naked ion (Emslie-Smith, 1988). The potential difference across the cell membrane will also prevent the iodine-ion (I^-) from entering the cell, because the intracellular potential is negative (Keele *et al*, 1982). It is therefore clear that the two iodine-123 carriers differ fundamentally with regard to their entry into cells.

1.2. Thesis objectives:

a. The first objective was to examine the cellular effects of iodine-123 offered as 4-[^{123}I]iodoantipyrine and as [^{123}I]NaI.

b. Secondly, to examine the effects of the decayed iodine-123 products on the cells.

c. Thirdly, to validate the uptake measuring techniques, using [^{201}Tl]TlCl, and then to determine the cellular uptake of iodine-123 as 4-[^{123}I]iodoantipyrine and as [^{123}I]NaI. The uptake rate of the two compounds and the kinetics of damage must be examined by different methods to asses the intracellular concentrations of 4-[^{123}I]iodoantipyrine and [^{123}I]NaI.

d. If the hypothesis is correct that 4-[^{123}I]iodoantipyrine readily enters the cell nucleus one would expect the benefit of Auger emission in the cell nucleus to be larger in the radioresistant cells than in the radiosensitive cells and the difference in radiosensitivity to diminish. The next objective therefore was to test this hypothesis by exposing a range of cell lines of differing radiosensitivity to 4-[^{123}I]iodoantipyrine. The [^{123}I]NaI experiments will serve the purpose to demonstrate the toxicity of Auger decay outside the cell.

e. If the direct action of radiation is the main mechanism for cell inactivation by Auger electrons, it can be hypothesised that radioprotective chemicals will be less effective for high-LET emitters, while scavengers will be more effective for [^{123}I]NaI which causes low-LET damage (Rao *et al*, 1990).

f. The final aim therefore is to compare the dose reduction factors (DRF's) of the radioprotector, DMSO, after 4-[^{123}I]iodoantipyrine and [^{123}I]NaI exposure.

CHAPTER 2: MATERIALS AND METHODS

2.1 Radionuclides and radioactivity counting

Carrier free [^{201}Tl]TlCl and [^{123}I]NaI were used as produced at the NAC. Uptake studies employed the K^+ analogue $^{201}Tl^+$, which is known to concentrate in cells (Kassis, 1994) and therefore provide a way of validating the methods. 4-[^{123}I]Iodoantipyrine was synthesised from [^{123}I]NaI, using a unique labelling technique developed at the NAC, as previously described (Slabbert *et al*, 1999) (see appendix for summary). A multichannel radioactivity counter was used and samples were placed at 6 cm from the open germanium detector.

2.2. Cell culture

Two murine cell lines, CHO-K1 and DMBA; two human cancer cell lines, A549 (lung carcinoma) and Nortje (hypernephroma); and two strains of AT (ataxia telangiectasia) cells, AT and ATs4, were used. These six cell lines were chosen, because they cover a wide range of radiosensitivity. Cells were grown as monolayers in: RPMI-1640 for the human cells, Ham's-F12 for the CHO-K1 and EMEM for the DMBA cells. All growth media were supplemented with 10% FCS and antibiotics (penicillin and streptomycin - 100 mg/l) and cells cultured at 37°C (5% CO_2 - 95% air). The cell culturing methods used are standard techniques generally used in radiobiology (Freshney, 1983) (All cell-culture chemicals: Highveld Biological, South Africa.)

2.3. Uptake experiments

Exponentially growing cells were trypsinised, washed and resuspended. Isotope uptake was examined by the following methods:

a. Triton-X method: Series of 4-5 duplicate samples of 0 to 60 x 10^3 CHO-K1 cells were seeded in 24x multiwell plates and the [^{201}Tl]TlCl, [^{123}I]NaI or 4-[^{123}I]Iodoantipyrine added when cells were attached. Plates were incubated for 18 hours and then placed on ice to minimise diffusion across the cell membranes. Radioactivity was removed by pasteur pipette and the monolayers of cells were washed twice with ice cold PBS. Then 1.5 ml of a 1% Triton-X soap solution was dispensed into each well. After 1 hour at 37 ^{o}C, to allow for dissolving of the cells, 1 ml from each well was transferred to eppendorf tubes and the radioactivity counted.

b. Silicon oil method: A variation of the Rapid Cell Filtration System as described by Capala *et al* (1996) to confirm Boron uptake in cells, was used to separate cells from the radioactive medium. Units of 1 ml of a mixture (8:2) of silicon oil (Dow Corning 550) and light mineral oil was placed in 2 ml centrifuge tubes. A series of 4-5 duplicate samples of [^{201}Tl]TlCl, 4-[^{123}I]Iodoantipyrine or [^{123}I]NaI was added to identical 1 ml CHO-K1 cell suspensions and incubated for 4 hours to allow radionuclide uptake. Volumes of 400 µl of these suspensions were then layered on top of the oil mixture. The density of the oil mixture was intermediate to the density of the suspended cells and the surrounding medium. When centrifuged at 12 000 rpm for 2 min, the layers stayed separated, but the cells penetrated through the oil mixture and pelleted in the tip of the tube. The centrifuge tube was placed in a lead jacket with only the tip exposed and the radioactivity associated with the cells was then counted, using a multichannel counter.

c. Spin-X filter method: The Spin-X® centrifuge filter (®Costar) contains a removable 0,22 μm cellulose acetate filter insert within a 2 ml centrifuge tube. A series of 3 duplicate samples of V79 cell concentrations were exposed to 4-[^{123}I]iodoantipyrine and [^{123}I]NaI and after 4 hours 400 μl of each sample was transferred to the filter insert in the tube. The tubes were centrifuged at 12 000 rpm for 7 min and this forced the supernatant medium through the filter. The cells accumulated on the filter and the dry filter units were removed and the radioactivity associated with the cells, measured. The Spin-X filter method requires a narrow cell concentration range to be successful. Too few cells ($< 250 \times 10^3$) do not give high enough readings to be distinguishable from the background and to many cells ($> 1500 \times 10^3$) clogs the filter and prevents it from spinning dry.

2.4. Possible chemical toxicity of the decayed compounds

The labelling status of iodine-123 to antipyrine was verified using a Waters Model 510 high-pressure liquid chromatograph (HPLC). The chemical effect of the 4-[^{123}I]iodoantipyrine on the cells was examined by allowing the 4-[^{123}I]iodoantipyrine to decay through ten half lives (< 0.001% of the initial activity) before adding it to the cells. To establish the percentage of deiodination, a HPLC purity analysis was again done after 10 half lives. A similar chemical concentration series of the 10 half lives old 4-[^{123}I]Iodoantipyrine, than the radioactive 4-[^{123}I]Iodoantipyrine, was added to DMBA cells.

The same methodology of exposure, radioactivity removal and cell seeding, as described in 2.6, was then followed and biological damage quantified using micronuclei counts.

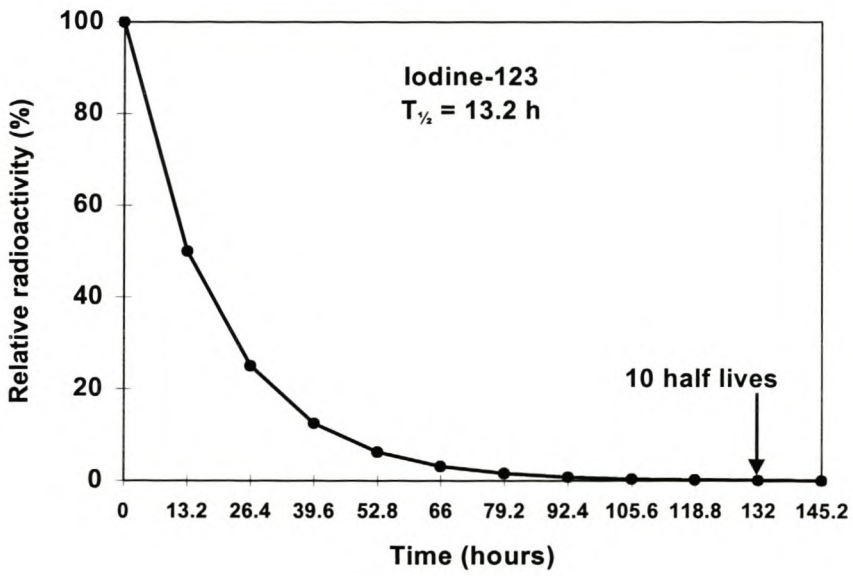

Fig. 2.1. Decay curve of iodine-123, showing that 0.001% of the initial activity will be left after 10 half lives (5.5 days).

2.5. Kinetics of damage

A delayed cellular uptake can have a significant influence on the toxicity of iodine-123. The uptake rate was examined by exposing similar numbers of CHO-K1 cells to a series of the same amounts of 4-[^{123}I]iodoantipyrine and [^{123}I]NaI for a range of varying times (0 - 190 min). The controls were not exposed to radioactivity. In the first samples in the range the 4-[^{123}I]iodoantipyrine and [^{123}I]NaI was added and the cell suspensions were centrifuged immediately and the radioactivity was removed to give a total exposure time of 7 min. The cells were then washed twice with growth medium to remove excess radioactivity and seeded for the micronucleus assay. The time series continued with increasing intervals up to 190 min for both the 4-[^{123}I]iodoantipyrine and [^{123}I]NaI.

2.6. Exposure to 4-[^{123}I]iodoantipyrine and [^{123}I]NaI

Exponentially growing cells of each of the six cell lines were trypsinized, suspended in calcium-free growth medium, diluted and divided into 1 ml aliquots containing about 150 x 10^3 cells each. The cell suspensions were kept in 10-ml test tubes and the radionuclides, made up in growth medium, was added by serial dilutions to obtain maximum concentrations of about 2.5 mCi/ml and 1.5 mCi/ml for [^{123}I]NaI and 4-[^{123}I]iodoantipyrine respectively. The tubes were incubated for 4 hours, to facilitate uptake of the radionuclide. After 4 hours of incubation, the cells were pelleted by centrifugation and the radioactive medium was removed by pasteur pipette. The cells were then re-suspended in complete growth medium and washed twice, before seeding onto coverslips in 35-mm petri dishes and culturing.

2.7. Micronucleus assay

The micronucleus assay was used to determine the radiation damage to the DNA (Almassy *et al*, 1987). After irradiation, Cytochalasin B was added at a final concentration of 4 µg/ml to arrest the division of the cells in the binucleated stage. This permits karyokinesis but inhibits cytokinesis. The time of culture ratio in

Cytochalasin B was related to the growth rate of the cell type. Slow growing cells required up to 60 hours of culturing time for a binucleated percentage of above 70%, compared to fast growing cells that typically only required about 24 hours of culture time. The cells were then fixed in a methanol, acetic acid mix (3:1) and stained with acridine orange. Micronuclei and main nuclei stained bright yellow and cytoplasm stained orange. Binucleated- and micronuclei-containing binucleated cells were examined using a 40x, oil immersion objective, in an UV-light equipped Zeis Axioscope. Micronucleus scoring was according to the criteria of Almassy *et al.* (1987). A micronucleus was scored if it had the same structure as the main nucleus; did not exceed half the size of the main nuclei; was round and clearly separated from the main nucleus and lay in well preserved intact cytoplasm.

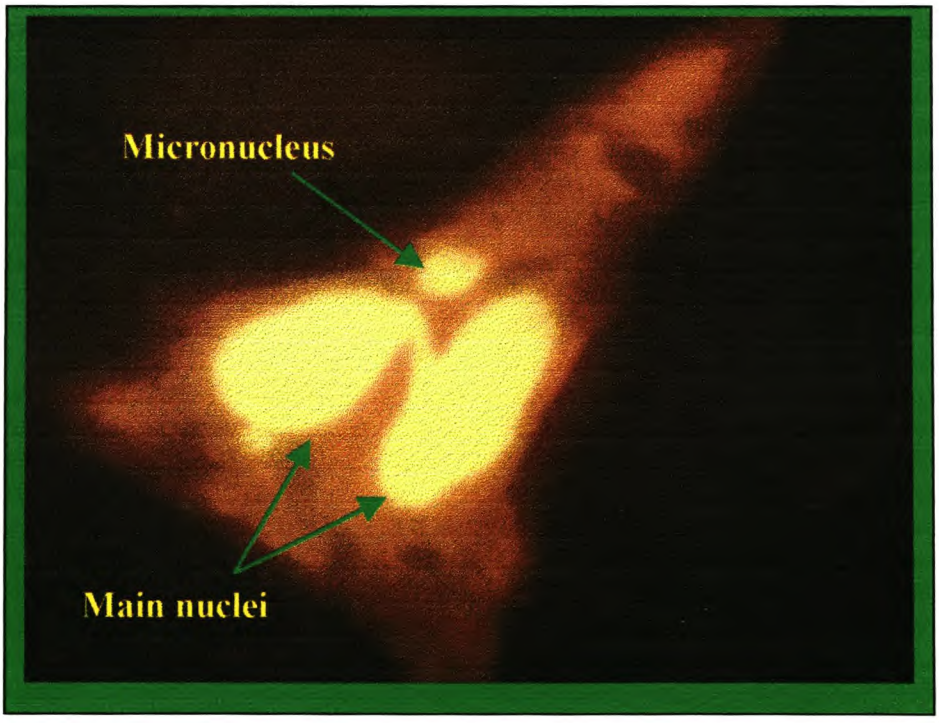

Fig. 2.2. Photomicrograph (630x) of a fluorescent image of an acridine orange stained binucleate cell, containing two micronuclei.

2.8. Radioprotection

The radioprotective effect of dimethyl sulphoxide (DMSO), an OH^- scavenger and cryoprotector, was examined. Four identical series of 5 single samples of suspended Nortje cell concentrations of about 150 x 10^3 cells/ml was prepared and DMSO was added to two of the sets to give a final DMSO concentration of 10% (v/v). 4-[^{123}I]Iodoantipyrine and [^{123}I]NaI was each added by serial dilutions to obtain a concentration of about 1.5 mCi/ml and 2.5 mCi/ml respectively, to a series with and without DMSO. The two sets containing DMSO were placed in a freezer (-20°C) and the sets with no DMSO were incubated at 37°C. Solid freezing of the samples at -20°C occurred within 30-60 min. All samples were left for 4 hours to allow for sufficient isotope disintegration. They were then taken out of the incubator and freezer and the frozen samples were defrosted in a 37°C water bath. Complete defrosting happened within 3 min and all samples were then centrifuged and the radioactivity removed. Cells were washed twice using growth medium and then seeded as for micronuclei counts.

2.9 Statistical analysis

Linear curves were fitted to all radionuclide uptake data and micronuclei frequency data. R^2 values are shown on the graphs or are tabulated. Error bars on micronuclei frequency data points indicate the standard deviation (S.D.). P-values are indicated where applicable. Statistical analysis was done using MS Excel Statistical Analysis Toolpack and GraphPad-Prizm.

CHAPTER 3: RESULTS

3.1 Radionuclide uptake

Radionuclide uptake was determined by the Triton-X, Silicon oil and Spin-X centrifuge filter methods using CHO-K1, CHO-K1 and V79 cells respectively. (Fig. 3.1-3.4). Total intracellular ^{201}TlCl measurements, plotted as a function of the number of CHO-K1 cells showed a good linear response for both the Triton-X and the Silicon oil methods (Fig. 3.1). A slightly lower response was observed with the Triton-X method compared to the Silicon oil method. The volume of a suspended CHO-K1 cell was measured as 2.027×10^{-6} µl. Figure 3.1 shows an intracellular ^{201}TlCl concentration of 2.083×10^{-5} µCi/cell. Since the cells were incubated in 0.74 µCi/µl, the intracellular enrichment factor escalates to 14.3. In contrast, cells exposed to [^{123}I]NaI showed no increase in total intracellular radioactivity with increasing cell numbers (Fig. 3.1). When the 4-[^{123}I]iodoantipyrine uptake was compared with [^{123}I]NaI uptake, using the Triton-X method, CHO-K1 cells showed a linear response of total intracellular 4-[^{123}I]iodoantipyrine with increasing cell numbers, compared to a flat response with [^{123}I]NaI for the range of 0 to 60×10^3 cells seeded (Fig. 3.2). The silicon oil method showed that uptake of 4-[^{123}I]iodoantipyrine into CHO-K1 cells in the range 0 to 250×10^3 cells, is 10 times higher than [^{123}I]NaI (Fig. 3.3). The Spin-X centrifuge filter method indicated accumulation of 4-[^{123}I]iodoantipyrine in Nortje cells by 5 times that of [^{123}I]NaI (Fig. 3.4).

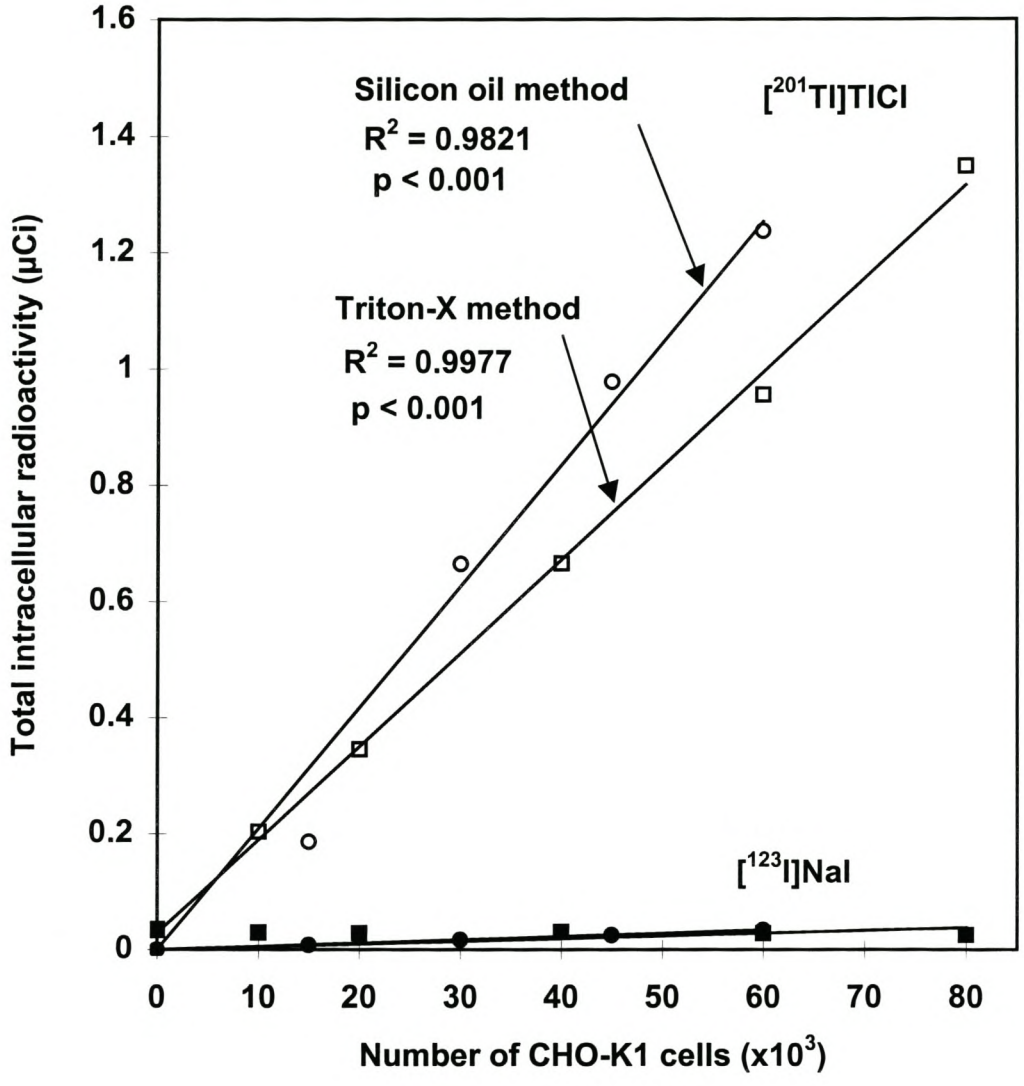

Fig. 3.1. Comparing uptake of [^{201}Tl]TlCl into CHO-K1 cells, using two different methods. Cells exposed to [^{123}I]NaI were used as control samples in each case.

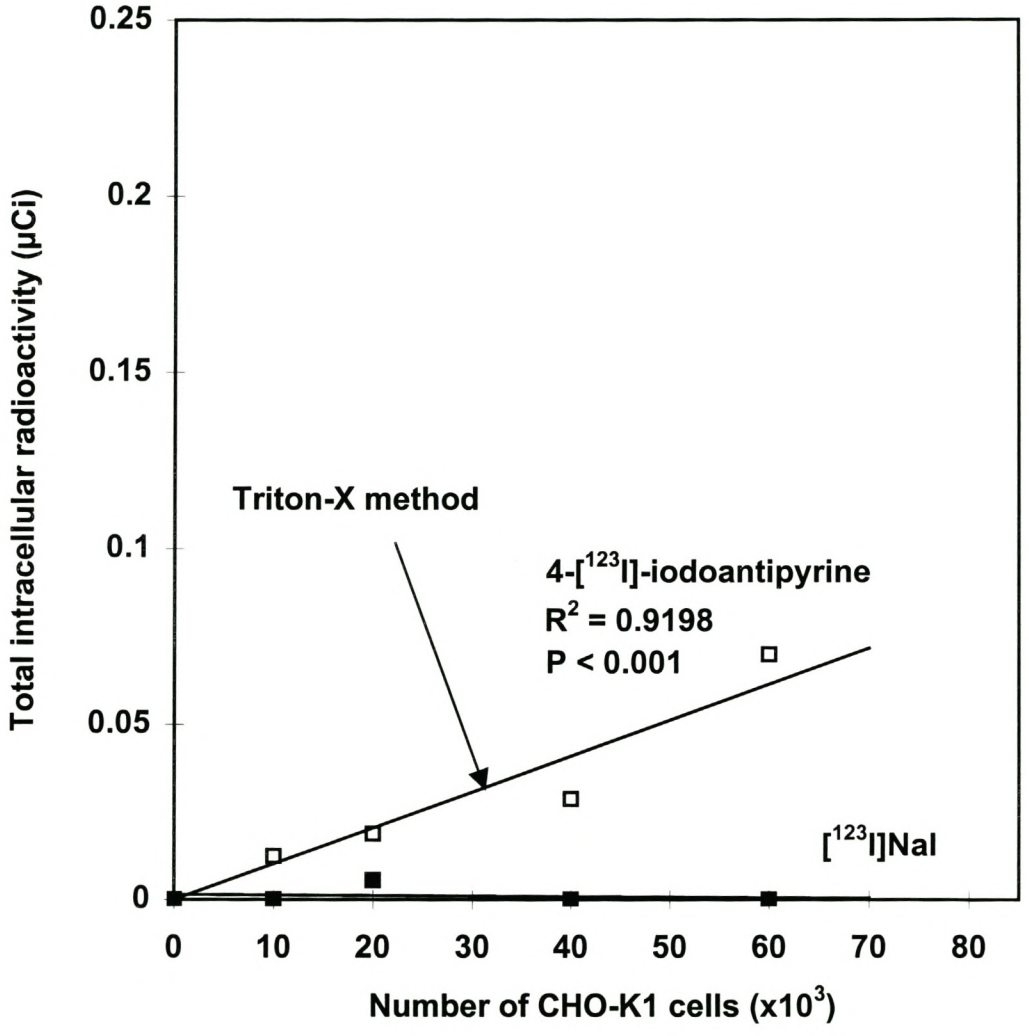

Fig. 3.2. Total intracellular 4-[^{123}I]-iodoantipyrine concentrations, using the Triton-X method, with cells exposed to [^{123}I]NaI used as control samples.

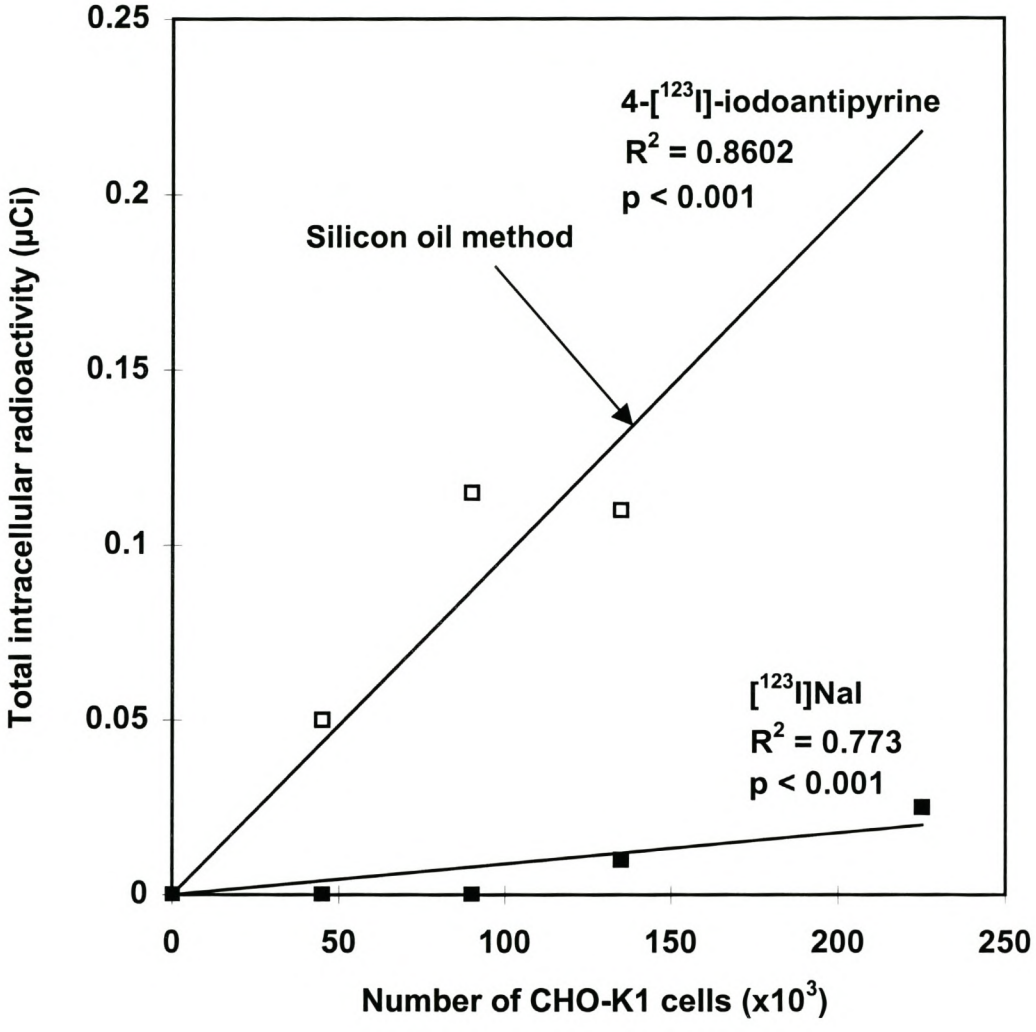

Fig. 3.3. Total intracellular 4-[^{123}I]-iodoantipyrine concentrations, using the Silicon oil method, with cells exposed to [^{123}I]NaI used as control samples.

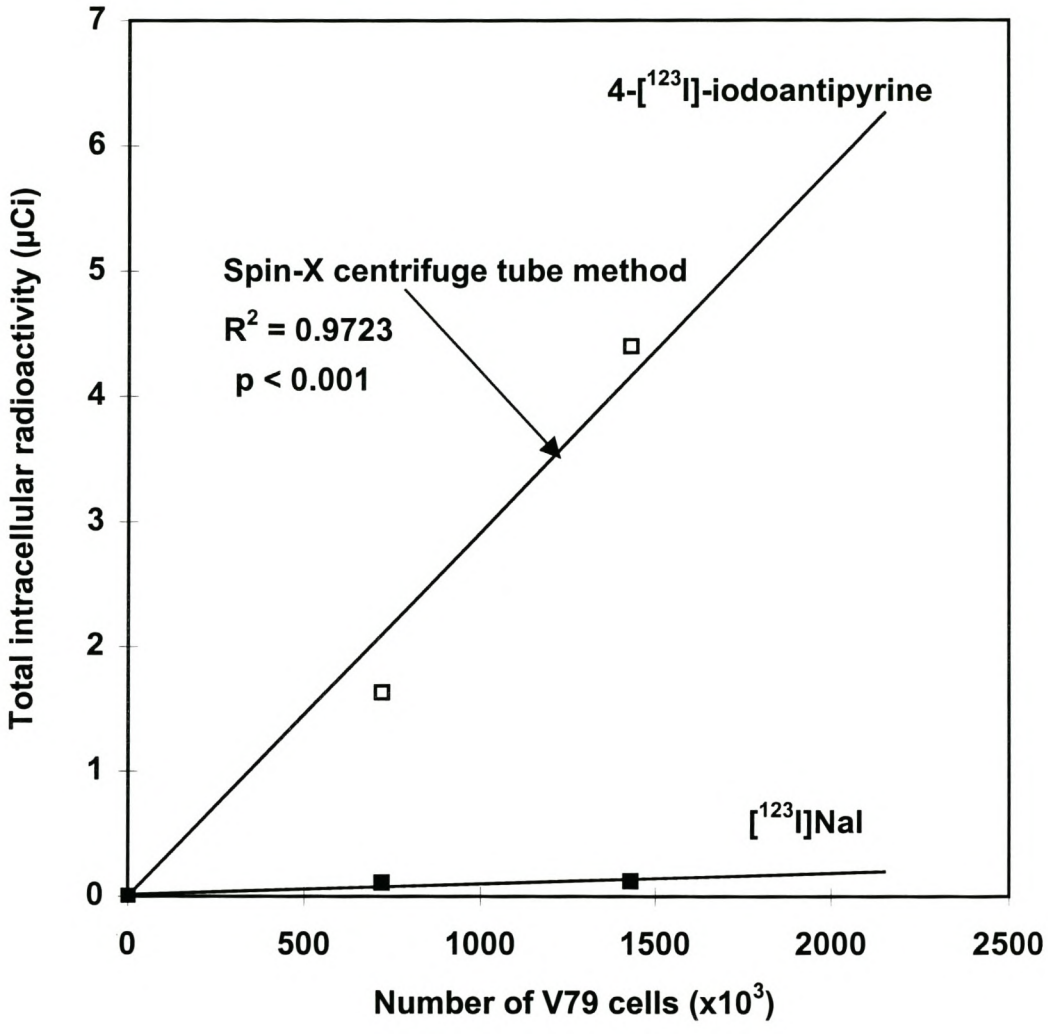

Fig. 3.4. Total intracellular 4-[^{123}I]-iodoantipyrine concentrations, using the Spin-X centrifuge tube filter method, with cells exposed to [^{123}I]NaI used as control samples.

3.2. Chemical toxicity of the decayed compounds

The HPLC graphs in fig. 3.5a+b demonstrate the labelling efficiency of iodine-123 to the antipyrine molecule. Peak number 1 on the HPLC graphs indicates the percentage of free (unlabelled) iodine-123 and peak number 2 represents the percentage of iodine-123 attached to antipyrine. A typical HPLC analysis after the synthesis of 4-[^{123}I]iodoantipyrine, routinely showed a > 98% purity (Fig. 3.5a). The equivalent chemical concentration of the radioactive 4-[^{123}I]iodoantipyrine added to the DMBA cells was calculated to be 11 nmol for each disintegration/μm^3. This is extremely low compared to the chemical concentration of a typical chemotherapeutic drug such as cis-Pt-II (Hall, 1988). For example, when cis-Pt-II is added at a concentration of 20 μmol to V79 cells for 1 hour, it will result in 37% cell survival (D_0). When active 4-[^{123}I]iodoantipyrine and [^{123}I]NaI were added to DMBA cells, dose response curves showed slopes of 527 (±32) and 293 (±23) respectively. In contrast, when decayed 4-[^{123}I]iodoantipyrine and [^{123}I]NaI were added to DMBA cells to give identical iodine (I^-) concentrations, no micronuclei response could be detected and a flat dose response curve was obtained (Fig. 3.6). The chemical influence of the added compounds therefore is negligible and does not contribute to the toxicity arising from the radioactivity. Deiodination of the iodine-123-labelled antipyrine was found to be ±7%, declining from >98% to 91%, over 10 half lives (Fig. 3.5b). This is not enough to influence the results. The chemical composition of the added substances therefore was essentially the same after 10 half lives, except for the fact that the iodine-123 had decayed.

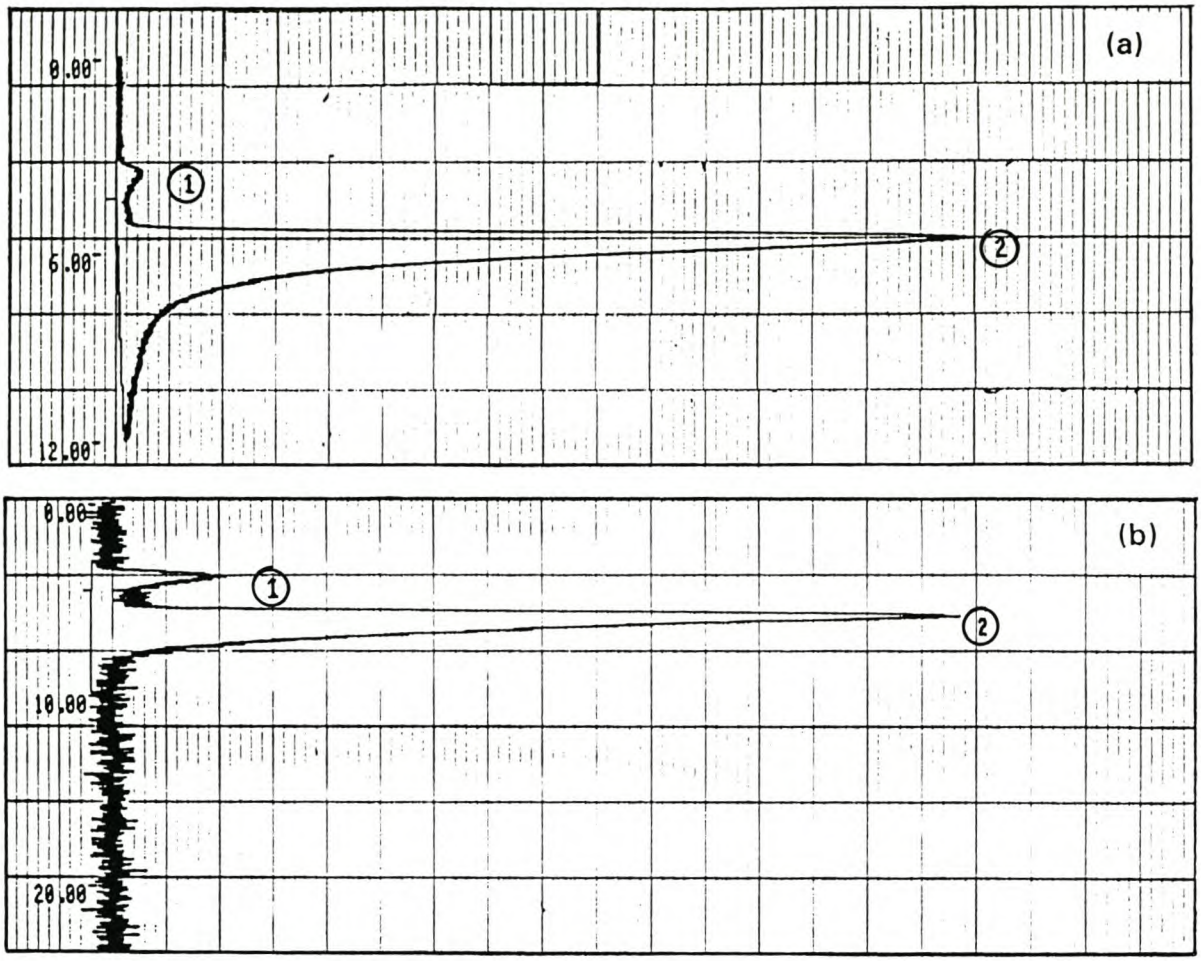

Fig. 3.5. HPLC graphs indicating the ratio between the iodine-123 labeled antipyrine (peak 2) and free iodine-123 (peak 1).

Fig. (a) demonstrates the purity analysis just after 4-[^{123}I]iodoantipyrine synthesis with 98% of the iodine-123 successfully labelled to antipyrine and 2% free iodine-123 present.

Fig. (b) represents the purity analysis 10 half lives after 4-[^{123}I]iodoantipyrine synthesis with only 0.001% of the initial activity left. It shows that 91% of the iodine-123 present was still labelled to antipyrine and 9% free iodine-123 was found.

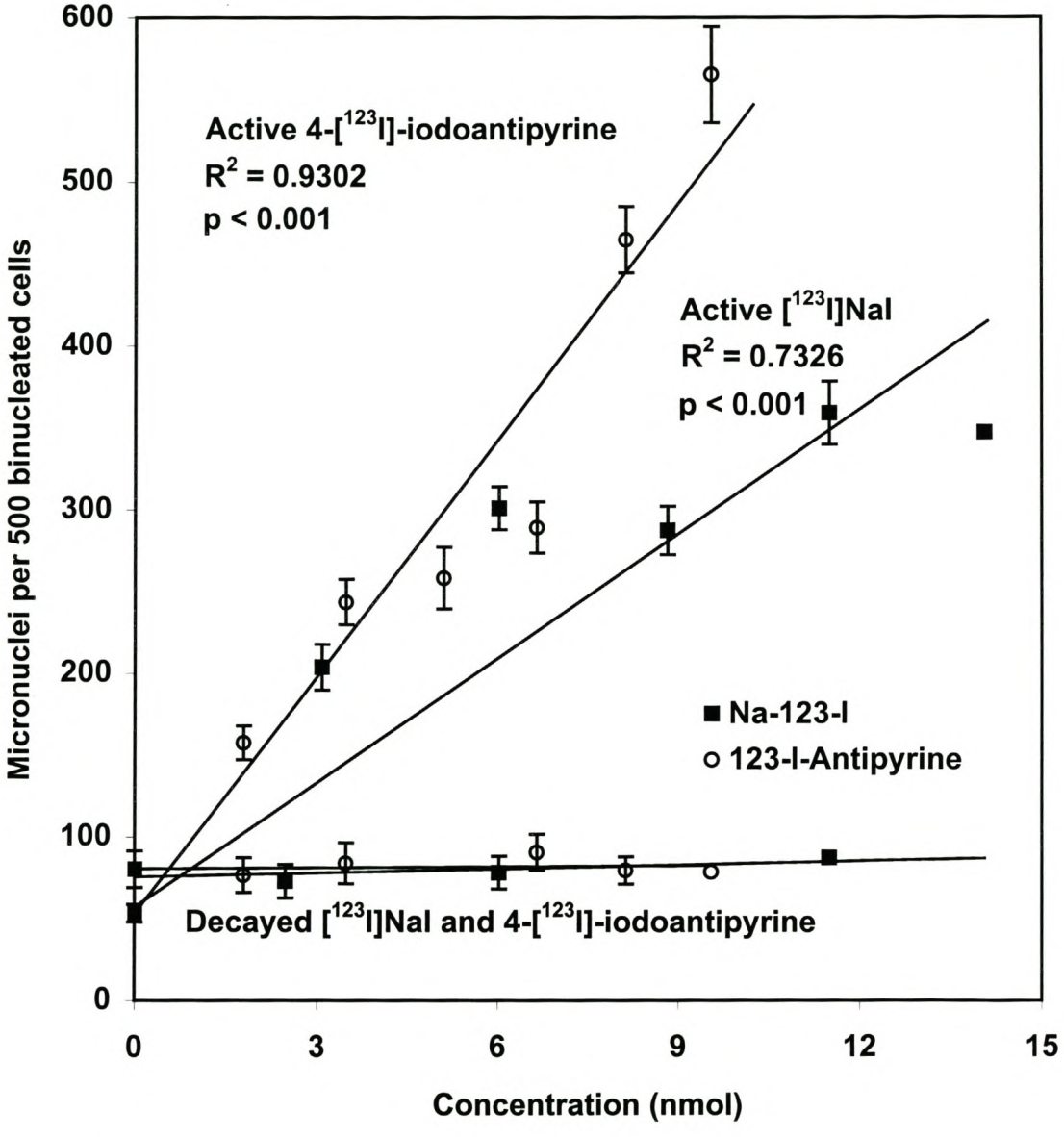

Fig. 3.6. Comparison between radioactive and decayed (10 half lives old) [^{123}I]NaI or 4-[^{123}I]-iodoantipyrine using DMBA cells

3.3. Kinetics of damage

The micronuclei frequency was found to increase linearly with time for both 4-[^{123}I]iodoantipyrine and [^{123}I]NaI (Fig. 3.7a). In the case of 4-[^{123}I]iodoantipyrine the increase in MN frequency was much higher than the MN frequency induced by [^{123}I]NaI. The slopes of the 4-[^{123}I]iodoantipyrine and [^{123}I]NaI lines are 1.30 (±0.04) and 0.70 (±0.05) respectively and therefore significantly different. (Fig. 3.7a). When the micronuclei frequency/disintegration/μm^3 was plotted as a function of total disintegrations/μm^3 for each exposure time, it showed two negatively sloped virtually parallel lines (Fig. 3.7b). These lines represent the trend in the MN frequency per unit dose over the total exposure time. The slopes of these 4-[^{123}I]iodoantipyrine and [^{123}I]NaI lines are -62 (±46) and -44 (±67) respectively with p-values of 0.27 and 0.56, which indicates that the slopes do not deviate significantly from zero. A negative trend on average is nevertheless clear for both lines. Extrapolation of the data to 0 disintegrations/μm^3 showed a high y-axis intercept for the 4-[^{123}I]iodoantipyrine line at 264 micronuclei/500BNC/disintegration/μm^3 and a lower intercept for the [^{123}I]NaI line at 155 micronuclei/500BNC/disintegration/μm^3. The ratio of the 4-[^{123}I]iodoantipyrine to the [^{123}I]NaI line was ±1.7 for all exposure times (Fig. 3.7b). This indicates the diffusion results of 4-[^{123}I]iodoantipyrine into the cells.

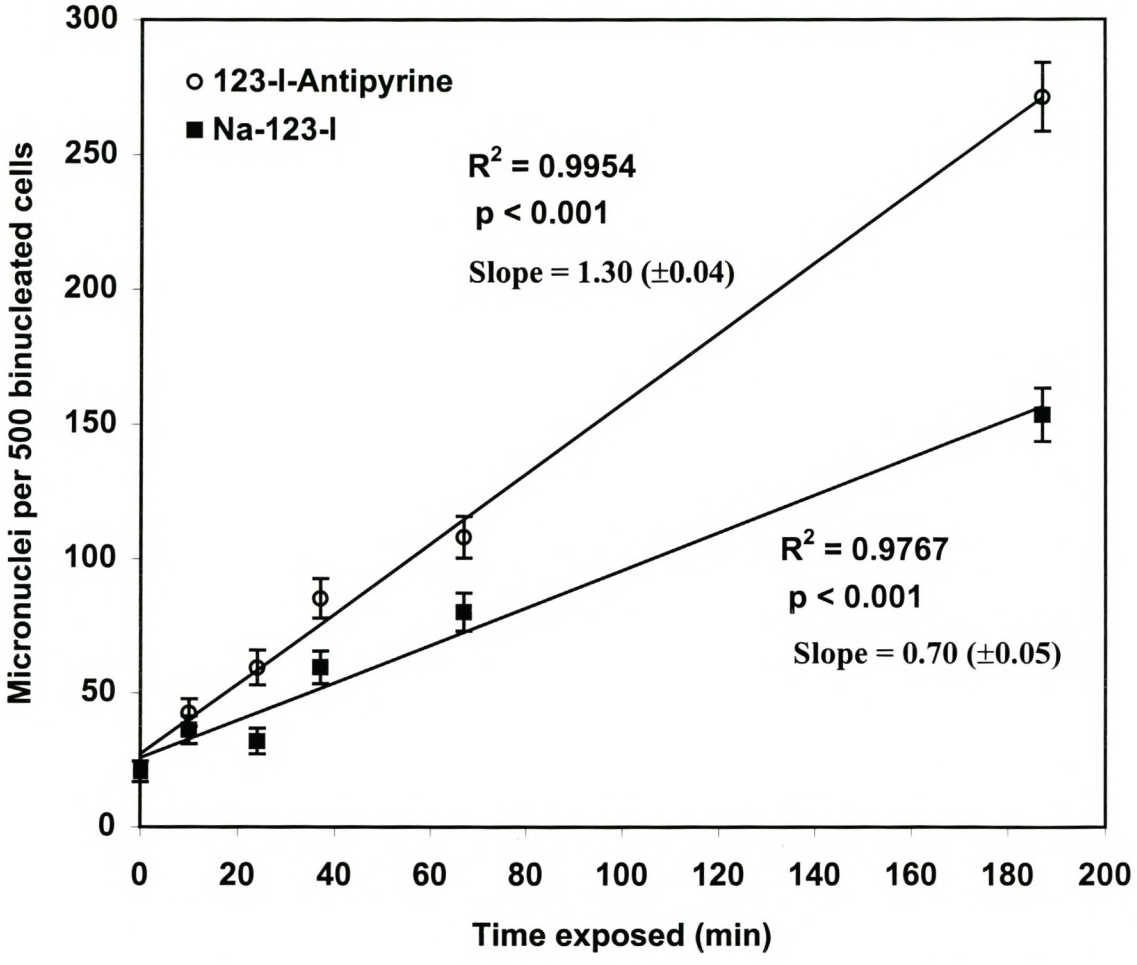

Fig. 3.7. (a) Micronuclei response in CHO-K1 cells as a function of exposure time to [^{123}I]NaI or 4-[^{123}I]iodoantipyrine.

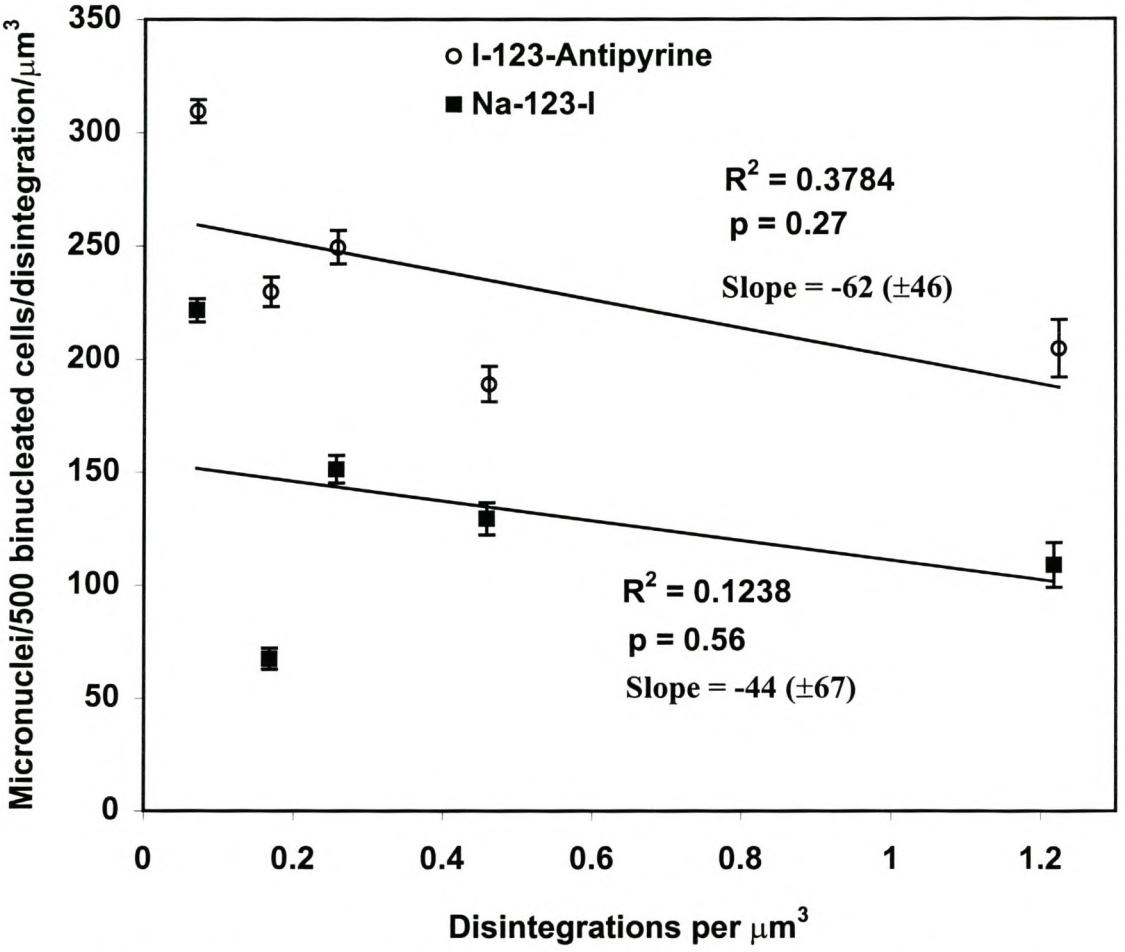

Fig. 3.7. (b) Micronuclei response in CHO-K1 cells exposed to [^{123}I]NaI or 4-[^{123}I]iodoantipyrine, expressed as micronuclei frequency (MN/500BNC) per unit dose (disintegrations/μm^3) as a function of total disintegrations/μm^3 for each exposure time.

3.4. Biological effects of 4-[^{123}I]iodoantipyrine and [^{123}I]NaI

When micronuclei frequencies were plotted as a function of disintegration per μm^3 of 4-[^{123}I]iodoantipyrine and [^{123}I]NaI, it was found that MN frequencies induced by 4-[^{123}I]iodoantipyrine was consistently steeper than that induced by [^{123}I]NaI. For A549 cells the slopes of the [^{123}I]NaI and 4-[^{123}I]iodoantipyrine dose response curves were 43 (±7) and 134 (±10) respectively. No overlap of error bars occurred and the curves therefore are statistically significantly different. Similarly the curves of ATs4, CHO, DMBA, Nortje and AT cells shows [^{123}I]NaI and 4-[^{123}I]iodoantipyrine slopes of 69 (±13) and 123 (±9), 213 (±11) and 334 (±17), 293 (±23) and 527 (±32), 239 (±18) and 698 (±9), 432 (±23) and 948 (±90) respectively. (Fig. 3.8-3.10). This indicates entry of 4-[^{123}I]iodoantipyrine into the cells and exclusion of [^{123}I]NaI. The slopes and standard errors of the linear dose response curves are listed in Table 3.1. The ratios between the slopes of the [^{123}I]NaI dose response curves for the two murine cell lines, the human cancer cell lines and the two strains of AT cell lines, are 1.38, 5.56 and 6.26 respectively. ^{60}Co γ-irradiation shows a similar range of radiosensitivities (Table 3.1). RBE values range from 1.6 to 3.1 (Table 3.1). No relationship is found between RBE plotted as a function of ^{60}Co slopes ($p = 0.96$) (Fig. 3.13) or between RBE and [^{123}I]NaI dose response curve slopes ($p = 0.65$) (Fig. 3.12). However, a good linear relationship (slope = 2.13 (±0.39), $R^2 = 0.883$) is found between 4-[^{123}I]iodoantipyrine and [^{123}I]NaI dose response curve slopes (Fig. 3.11).

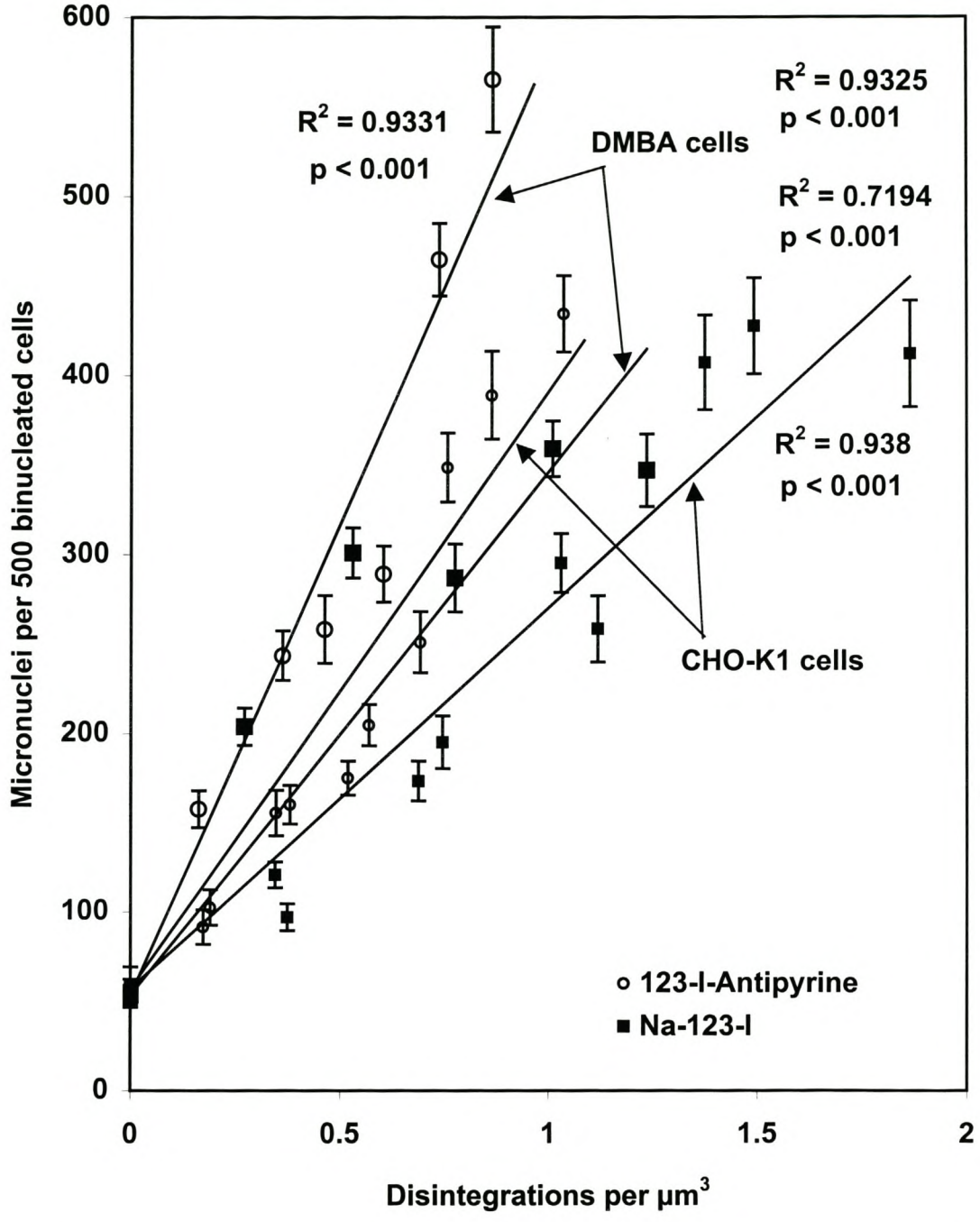

Fig. 3.8. Evaluation of the micronuclei response after exposure of CHO-K1 and DMBA cells to [^{123}I]NaI or 4-[^{123}I]-iodoantipyrine.

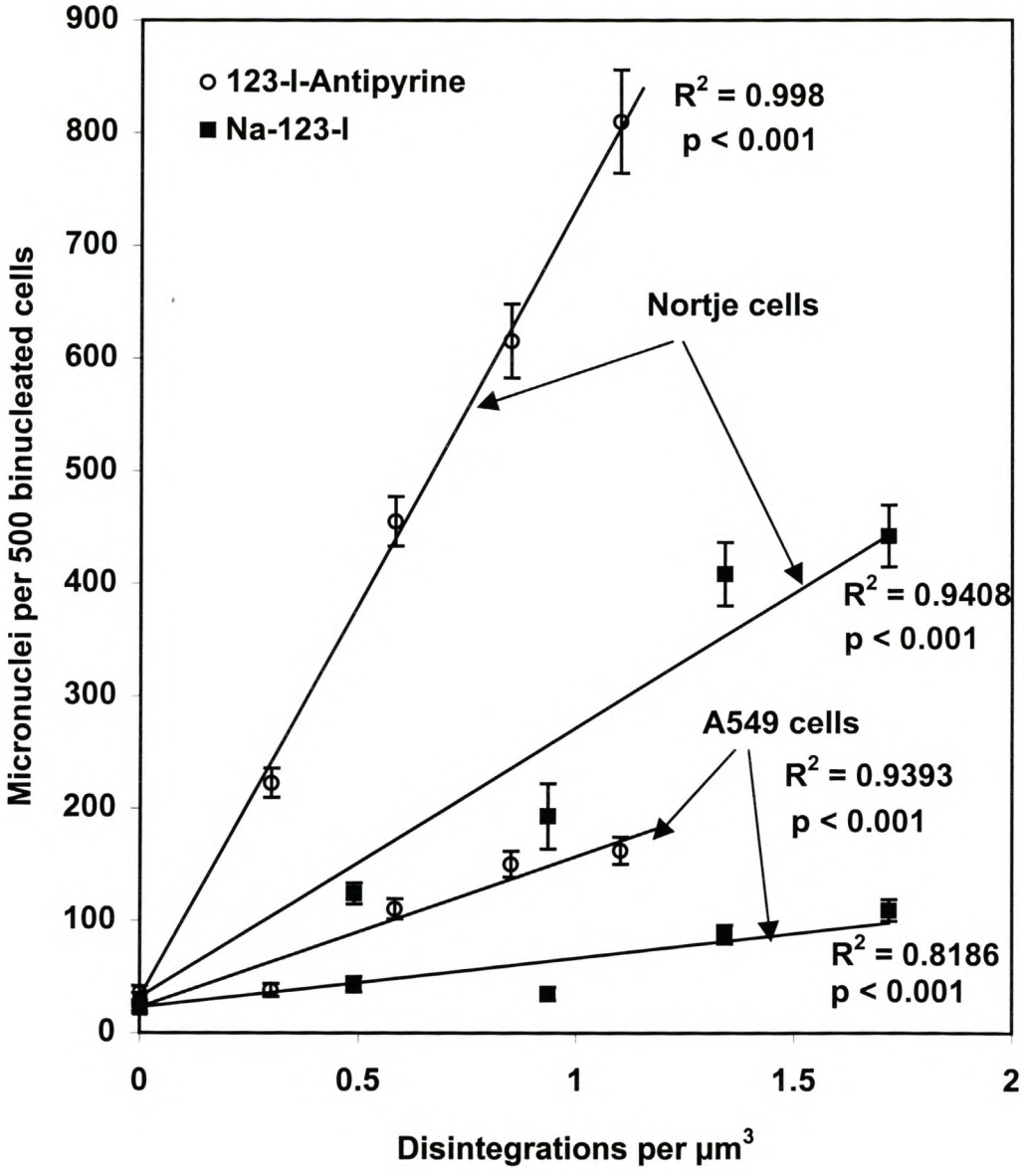

Fig. 3.9. Evaluation of the microruclei response after exposure of Nortje and A549 cells to [^{123}I]NaI or 4-[^{123}I]iodoantipyrine.

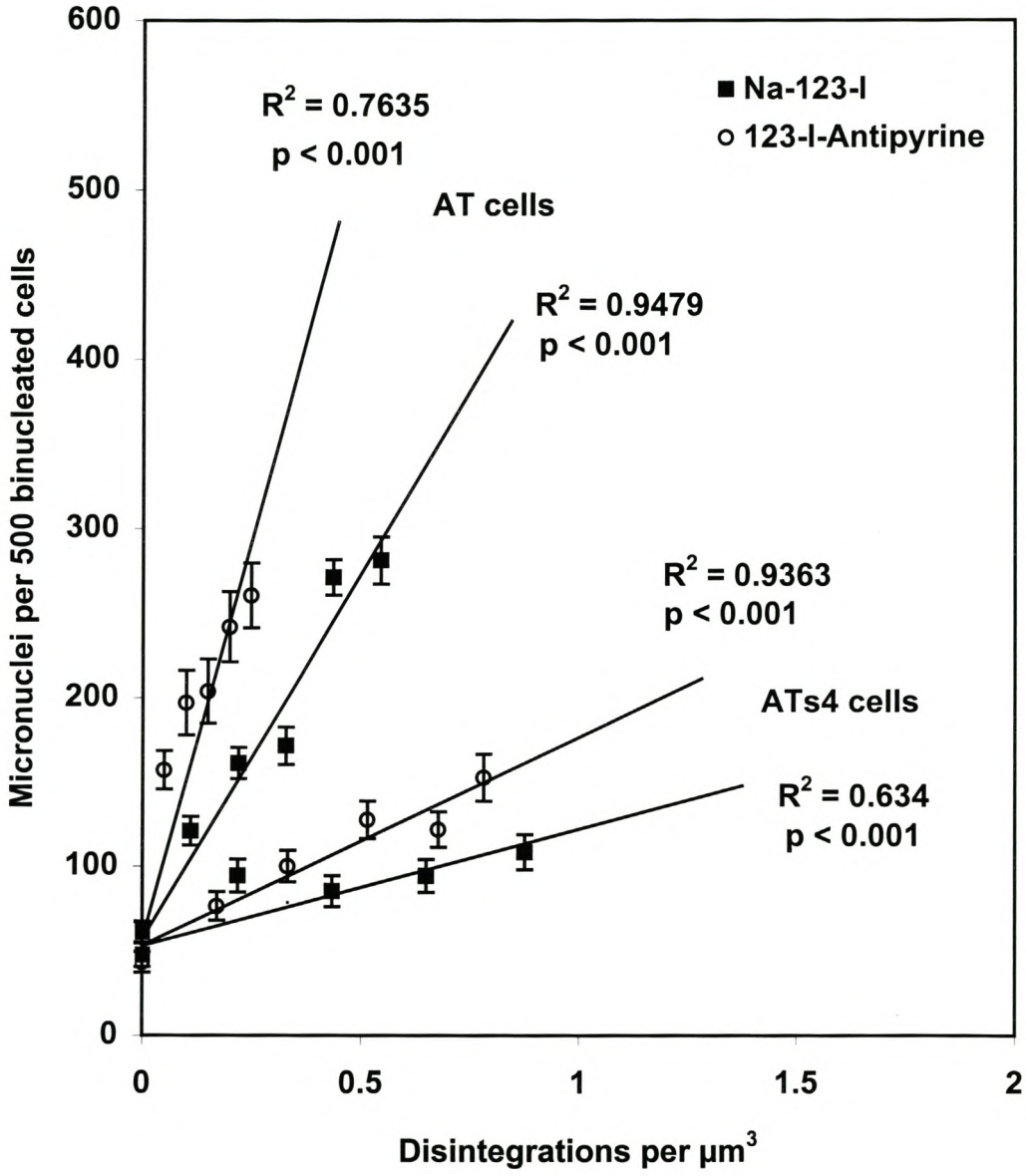

Fig. 3.10. Evaluation of the micronuclei response after exposure of AT and ATs4 cells to [^{123}I]NaI or 4-[^{123}I]-iodoantipyrine.

Cell line	Micronuclei frequency (MN/500BNC) per disintegration/μm^3 (Slope of dose response curves)					
	^{60}Co	[^{123}I]NaI	R^2	^{123}I-Antipyrine	R^2	RBE
A549	35	43 (±7)	0.819	134 (±10)	0.939	3.1
ATs4	76	69 (±13)	0.634	123 (±9)	0.936	1.8
CHO	51	213 (±11)	0.938	334 (±17)	0.933	1.6
DMBA	105	293 (±23)	0.719	527(±32)	0.933	1.8
Nortje	130	239 (±18)	0.941	698 (±9)	0.998	2.9
AT		432 (±23)	0.948	948 (±90)	0.764	2.2

Table 3.1. Micronuclei frequencies (MN/500BNC) per disintegration/μm^3 in six cell lines, ordered according to increasing radiosensitivity (as indicated by a 2 Gy ^{60}Co γ-dose), comparing the dose response curves of 4-[^{123}I]iodoantipyrine and [^{123}I]NaI to establish a RBE.

Note: The RBE is described as the ratio of the 4-[^{123}I]iodoantipyrine slope to the [^{123}I]NaI slope.

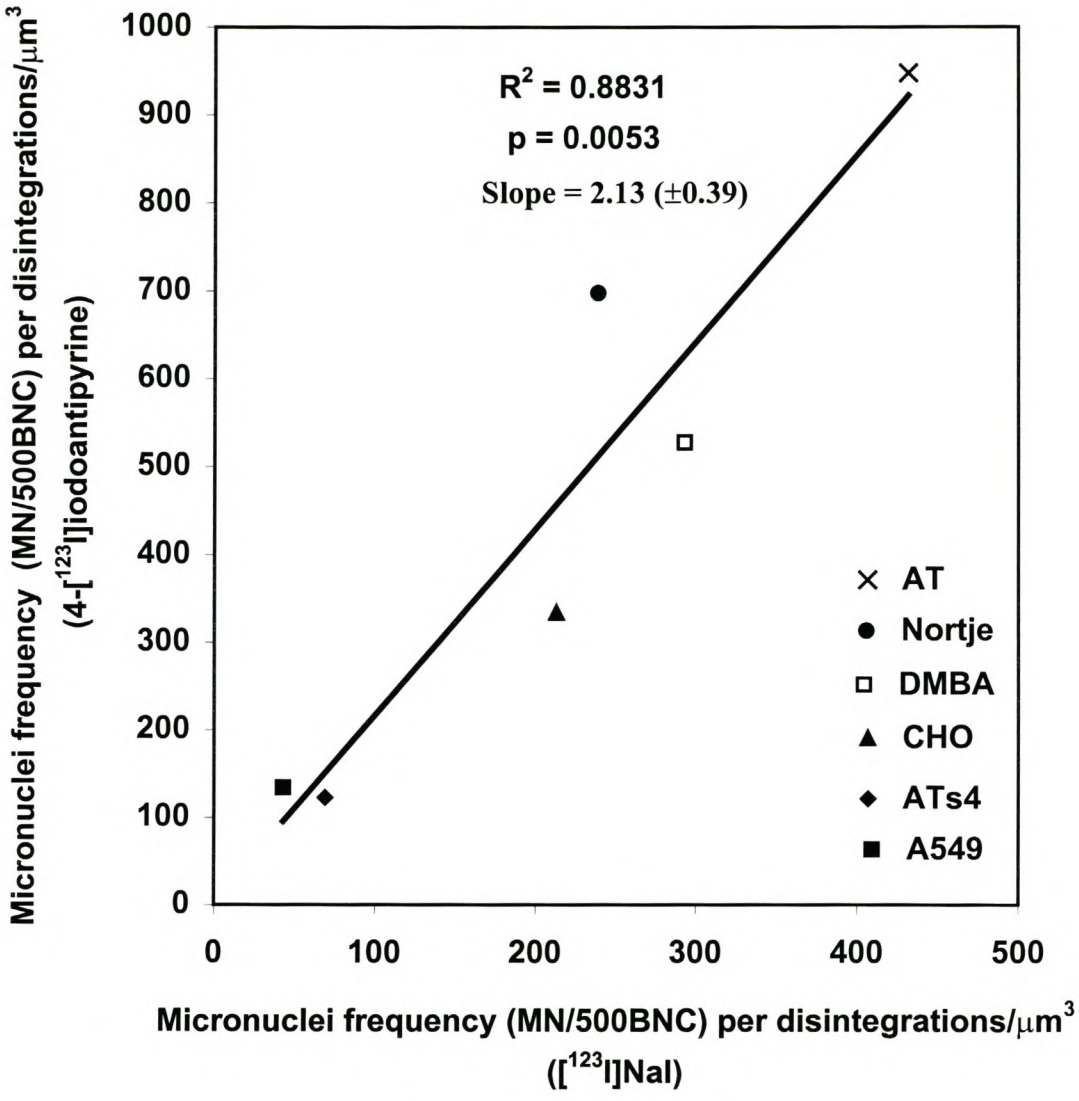

Fig.3.11. Micronuclei frequency/disintegration/μm^3 observed in various cell types after exposure to 4-[^{123}I]iodoantipyrine, plotted as a function of micronuclei frequency /disintegration/μm^3 seen after [^{123}I]NaI exposure.

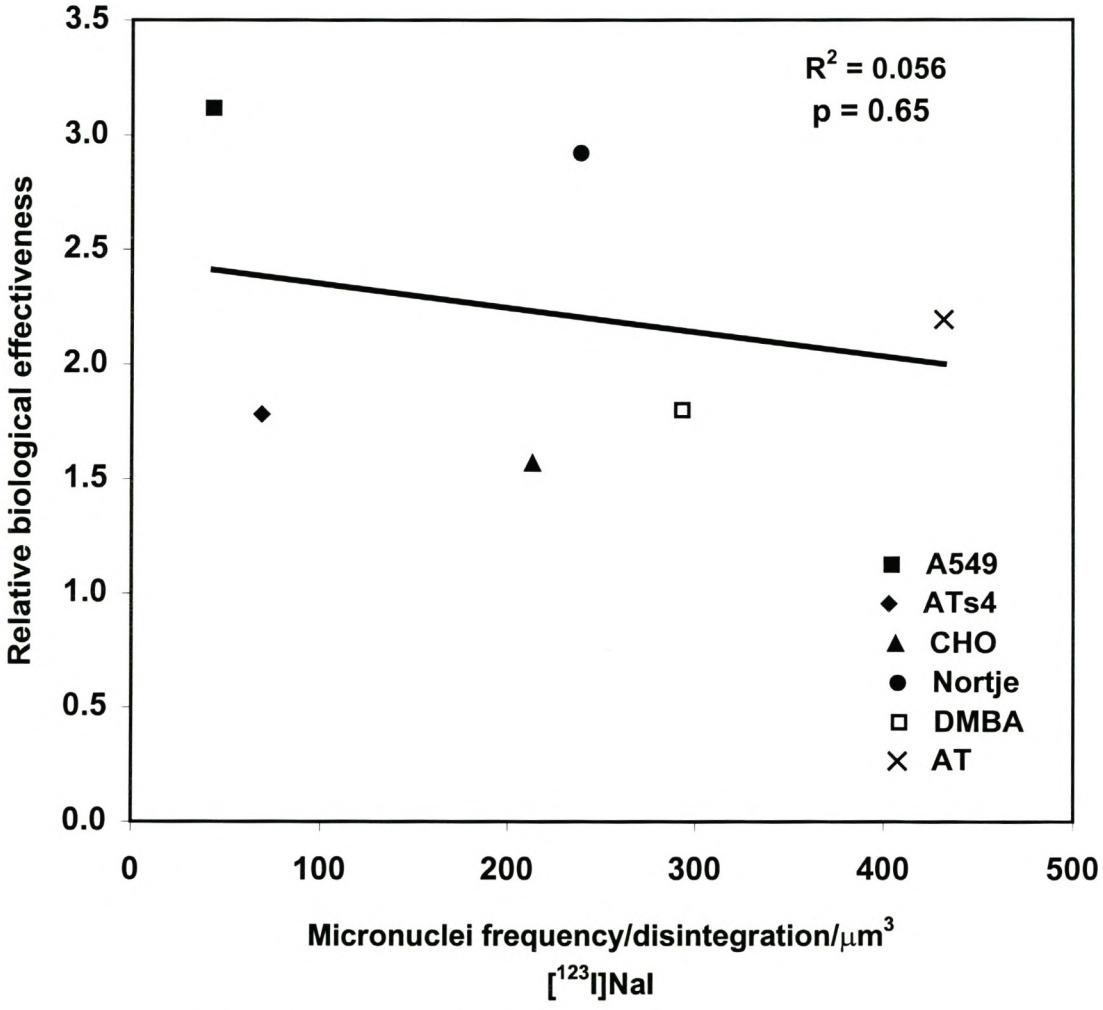

Fig. 3.12. The relative biological effectiveness of 4-[^{123}I]iodoantipyrine (relative to [^{123}I]NaI) in six cell lines, as a function of radiosensitivity as indicated by the micronuclei frequency/disintegration/μm^3 with [^{123}I]NaI exposures.

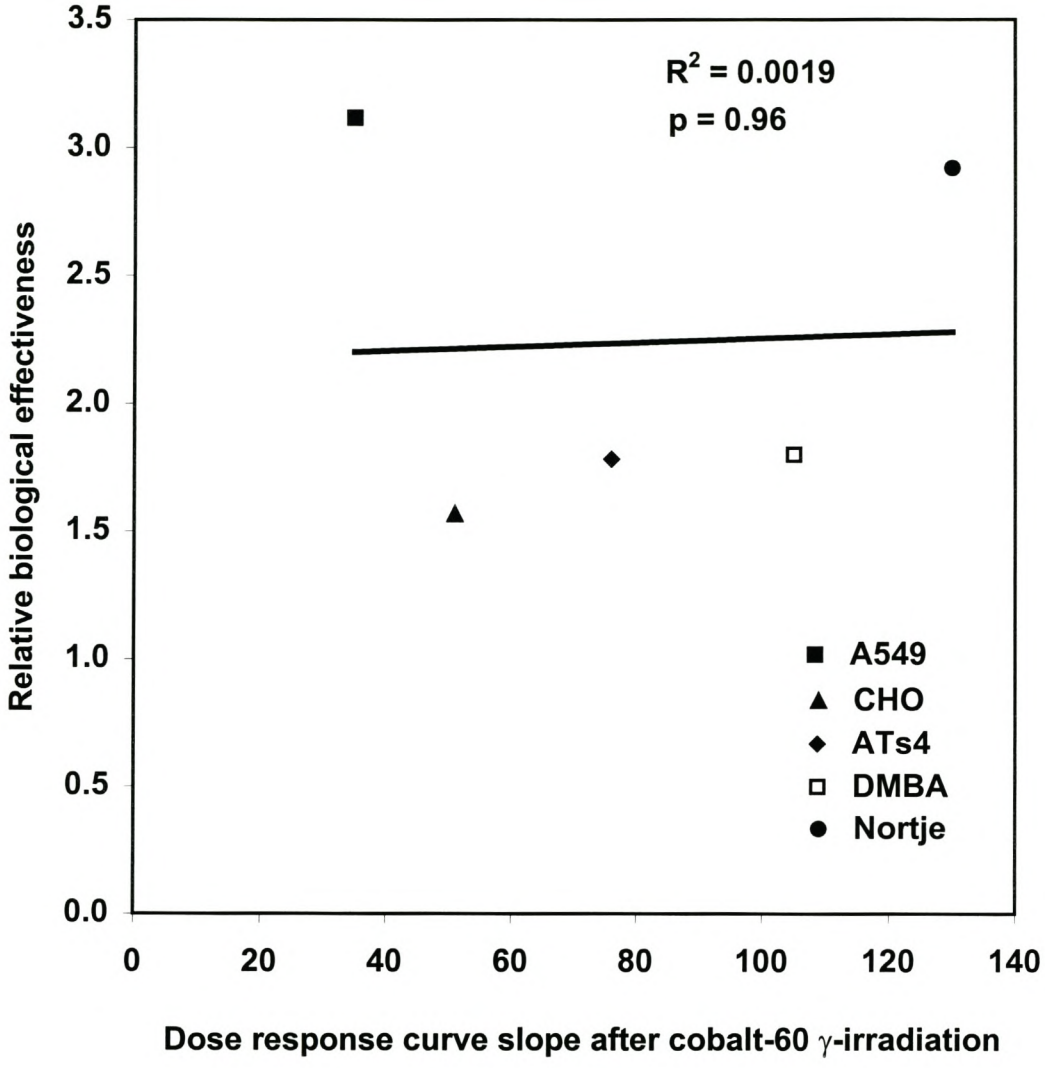

Fig. 3.13. The relative biological effectiveness of 4-[^{123}I]iodoantipyrine (relative to [^{123}I]NaI) in five cell lines, as a function of radiosensitivity as indicated by the dose response curve slopes with cobalt-60 γ-irradiation.

3.5. Radioprotection during cell freezing

The MN frequency in Nortje cells, obtained after exposure to the iodine-123 compounds in DMSO, and the MN frequency due to exposure under normal physiological conditions and in the absence of DMSO, is shown in figure 3.14. For 10% DMSO a dose reduction factor (DRF) of 1.29 and 1.24 was observed for 4-[^{123}I]iodoantipyrine and [^{123}I]NaI respectively (Table 3.2). The [^{123}I]NaI and 4-[^{123}I]iodoantipyrine slopes for no DMSO added were 266 (±18) and 455 (±16) respectively and showed no overlap of standard errors and is therefore significantly different. Similarly the 4-[^{123}I]iodoantipyrine and [^{123}I]NaI slopes for 10% DMSO added were 214 (±32) and 354 (±22) and are also statistically significantly different. For exposure with or without 10% DMSO the relative biological effectiveness (RBE) for 4-[^{123}I]iodoantipyrine (relative to [^{123}I]NaI) therefore was 1.65 and 1.71 respectively (Table 3.2.). Propagating the errors around the slopes in the RBE calculation produced RBE values for '10% DMSO' and 'no DMSO' of 1.65 (±0.3) and 1.71 (±0.15). These differences are statistically not significant and give no indication of the high-LET radiation effect expected for 4-[^{123}I]iodoantipyrine.

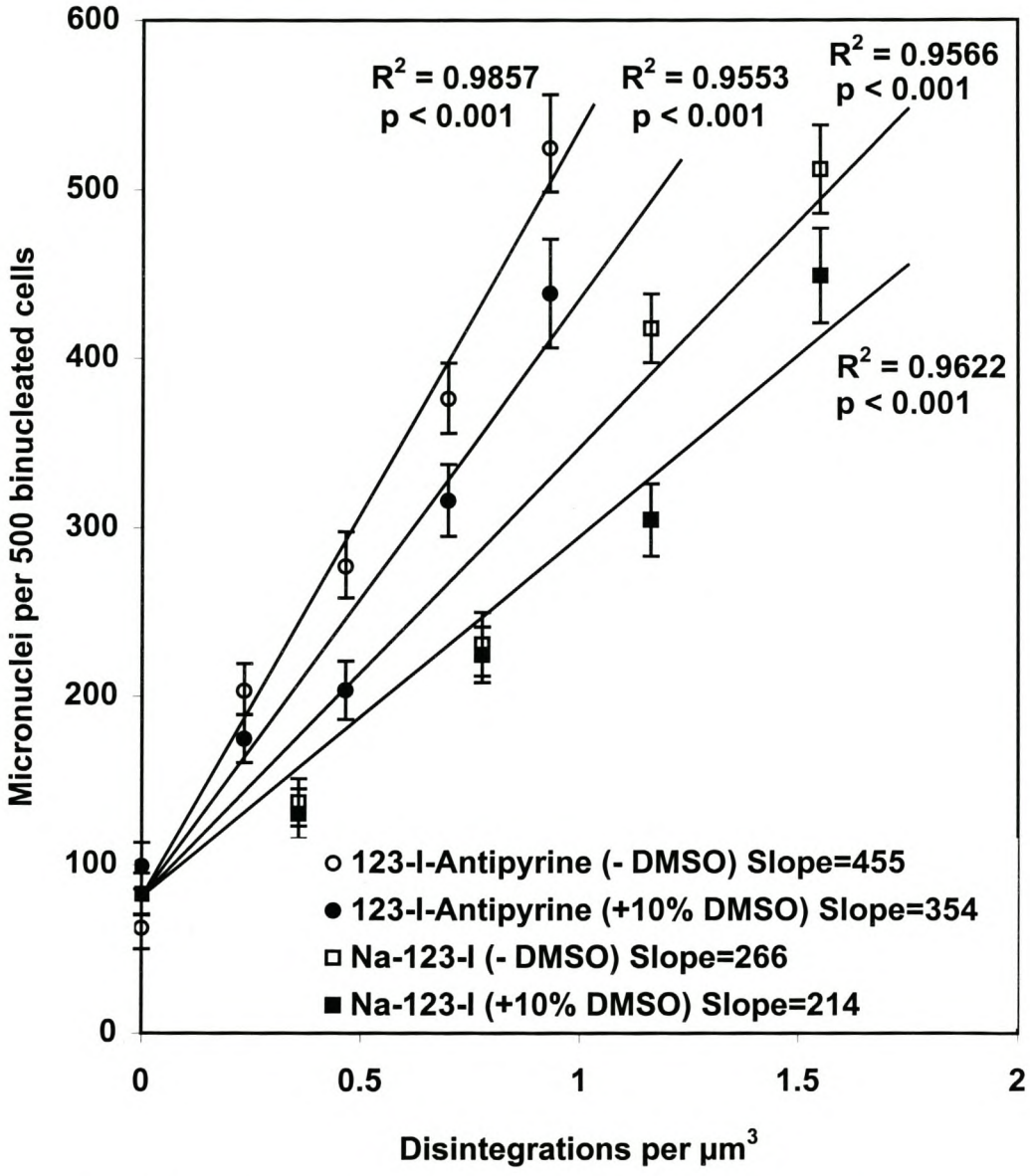

Fig. 3.14. Evaluation of the micronuclei response after exposure of Nortje cells to [^{123}I]NaI or 4-[^{123}I]-iodoantipyrine with and without the presence of 10% DMSO.

Iodine-123 compounds	Dose response curve slopes				DRF
	No DMSO	R^2	+10% DMSO	R^2	
^{123}I-Antipyrine	455 (±16)	0.986	354 (±22)	0.955	1.29
[^{123}I]NaI	266 (±18)	0.957	214 (±32)	0.963	1.24
RBE	1.71 (±0.15)		1.65 (±0.3)		

Table 3.2. Dose response curve slopes obtained after exposure of Nortje cells to 4-[^{123}I]iodoantipyrine or [^{123}I]NaI with and without the presence of DMSO. The dose reduction factors for DMSO and the RBE of 4-[^{123}I]iodoantipyrine compared to [^{123}I]NaI are also shown.

3.6. Modelling of DNA damage in chromatin

The influence of Auger electrons on DNA must take into account that the nucleus is composed of chromatin. In chromatin DNA and histones are associated in a 1:1 weight ratio, and are tightly organised into repeats of nucleosomes. The nucleosomes are linked by linker DNA to give a nucleosome chain of 11 nm in diameter which folds into solenoids of 32 nm diameter, 200 nm folded loops and 700 nm chromatids seen in mitotic chromosomes (Stryer, 1988). It is important to realise that the 11 nm nucleosome particle contains 2 x 2 nm of DNA-wraps and a central octomer histone complex of approximately 7 nm in diameter. See figure 3.15. If one assumes 3 arbitrary Auger tracks hitting a solenoid, it is clear that the target consists of DNA and histone density which alternate as sketched in figure 3.16 from Mathews and Van Holde (1990). From the tracks it becomes clear that Auger electrons cannot possibly hit DNA alone wherever they start. Regular and irregular DNA histone sandwiches occur which have to be traversed by the Auger electrons. In addition there are voids (fig. 3.16) which contain water. From the above it is not surprising that Auger decay is not restricted to the DNA only. (See discussion)

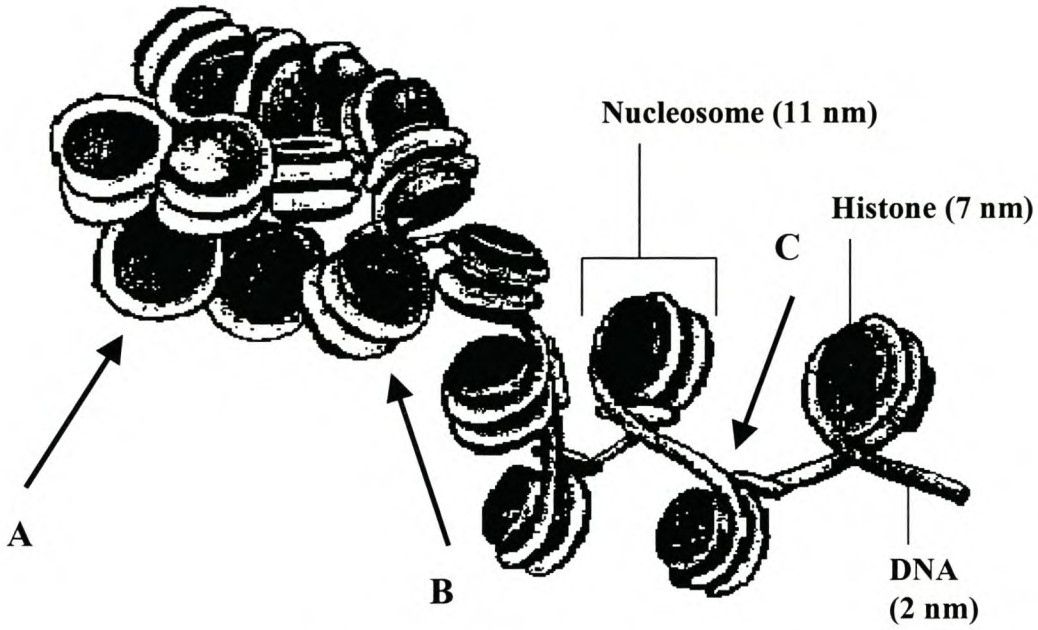

Fig. 3.15. Side view of chromatid solenoid showing three assumed Auger electron tracks (A, B and C) (Mathews and Van Holde, 1990).

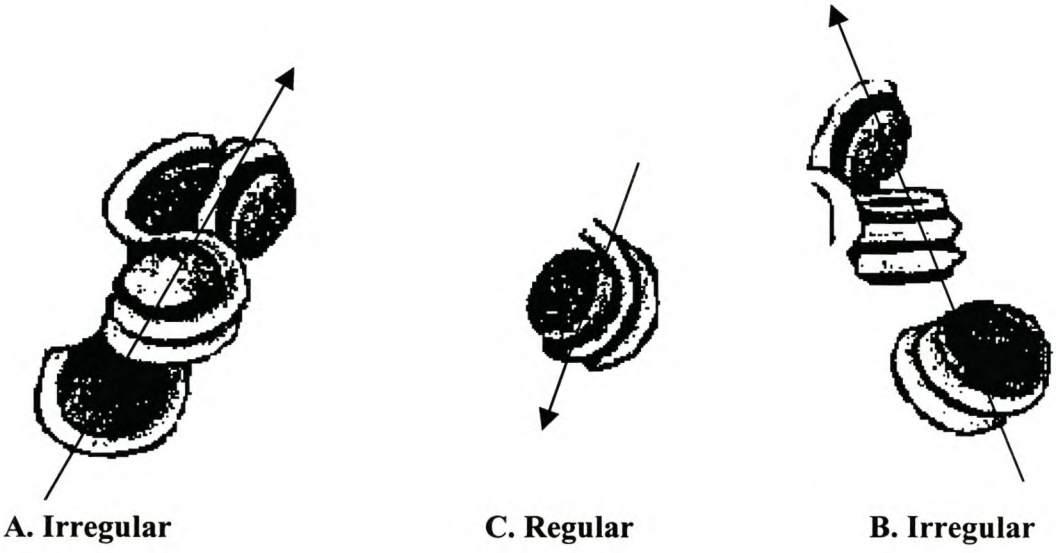

Fig. 3.16. DNA and protein density represented in three assumed Auger electron tracks through a chromatid solenoid (Mathews and Van Holde, 1990).

CHAPTER 4: DISCUSSION

After 10 half lives the chemical composition of the iodine-123 labelled antipyrine is stable and was found to be 91% (Fig. 3.5). This confirms that deiodination was insignificant. The lack of MN response after exposure to the decayed 4-[^{123}I]iodoantipyrine and [^{123}I]NaI shows that chemical effects could not be the explanation for the toxicity of these two iodine-123 carriers (Fig. 3.6). The flat dose response curves for both the decayed 4-[^{123}I]iodoantipyrine and [^{123}I]NaI shows this very clearly. The damage observed in the cells after exposure to active 4-[^{123}I]iodoantipyrine and [^{123}I]NaI can therefore only be ascribed to radiation effects. However, equal amounts of iodine-123 added to the cells in the form of 4-[^{123}I]iodoantipyrine or [^{123}I]NaI showed 4-[^{123}I]iodoantipyrine to be more effective. This very steep 4-[^{123}I]iodoantipyrine response curve as compared to the [^{123}I]NaI response, consistently seen in all cell lines, strongly suggests an Auger electron effect for the more effective agent (Fig. 3.8-3.10).

Three methods were used to measure intracellular radioactivity concentration. The results show that 4-[^{123}I]iodoantipyrine is preferentially taken up into the intracellular volume as compared to [^{123}I]NaI (Fig.3.2-3.4). In all three methods replicate measurements showed wide variations and it was not possible to relate the physical uptake to the induced toxicity. The highly diffuseable nature of antipyrine and the small intracellular concentrations of iodine-123 proved problematical. Washing of cells to remove unutilised isotope led to enormous losses. The same problem was noted by Kassis *et al* (1999).

The clonogenic assay is the gold standard of radiobiological analysis (see appendix). Radiosensitivity as determined by this assay is regarded as a reflection of mitotic integrity and true cell survival (Guo *et al*, 1998). Cell death derived from clonogenic assays can be due to necrosis, apoptosis and nondividing cells in G_0. MN formation reflects DNA (chromosome) damage and will not necessarily rank cells in the same order of radiosensitivity as the clonogenic assay (Guo *et al*, 1998). Akudugu *et al*,

(1999, in print) reported that MN formation should be viewed as a snapshot of DNA damage and not as a true reflection of remaining reproductive integrity. The amount of dose that could be delivered to the cells by exposure to [^{123}I]NaI or 4-[^{123}I]iodoantipyrine was restricted by the specific activity (mCi/ml) of iodine-123 in the cell suspension. The maximum specific activity that could be achieved resulted in approximately 1MN/BNC. This equates to ±37% survival (D_0) in colony assays and is not enough to construct a complete survival curve. The colony assay therefore could not be used to assess cellular damage from iodine-123 exposure. The exact dose that is delivered during disintegration of iodine-123 is uncertain and the MN data from iodine-123 exposure experiments could therefore not be compared with cobalt-60 colony assays. However, the MN assay is sensitive at low dose and was used to assess radiation damage (Ono *et al*, 1994). The steepness of the dose response curve was used as measure of radiosensitivity. A steep dose response curve and a rapid increase of micronuclei frequency suggest a more radiosensitive cell line (Fig. 3.8-3.10, Table 3.1).

Radionuclide exposure in the order of 4 hours was used to exclude the effects of cell division. This time was expected to be sufficient for iodine-123 entry into the nucleus. However, differences in uptake kinetics could not be excluded (Ludwikow *et al*, 1992). Diffusion of 4-[^{123}I]iodoantipyrine into the cells was found to be rapid. This is confirmed by the micronuclei frequency obtained at various isotope exposure times (Fig. 3.7a+b). The difference in MN frequency after exposure to 4-[^{123}I]iodoantipyrine or [^{123}I]NaI was already apparent at the shortest exposure time (Fig. 3.7a). The amount of damage per unit dose (disintegrations/μm^3) can be expected to be the same for all exposure times. However, figure 3.7b shows a definite downward trend on average for both 4-[^{123}I]iodoantipyrine and [^{123}I]NaI, while a flat horizontal relationship was expected. The dose rate for iodine-123 decay is the same for both iodine-123 carriers. Because of the short half-life (13.2 h) of iodine-123, the average dose rate in cells exposed for a short time would be higher than the average dose rate for a long exposure time. A reduction of the dose

rate change resulting from isotope decay (fig. 3.7b), shows that the damage/unit-dose is not constant. In view of the larger exposure times required for larger doses, it is suspected that repair may have played a role and induced the downward trends (fig. 3.7b).

The steeper micronuclei dose response after exposure to 4-[^{123}I]iodoantipyrine indicates that the iodine-123 in the form of 4-[^{123}I]iodoantipyrine is much more toxic than iodine-123 in the form of [^{123}I]NaI (Fig. 3.8-3.10). The reason for [^{123}I]NaI to be less toxic than 4-[^{123}I]iodoantipyrine can be attributed to the fact that [^{123}I]NaI does not enter the cells and nuclei (Kassis and Adelstein, 1980) and that the nuclide iodine-123 does not come close to the DNA. The toxic effects seen after exposure to [^{123}I]NaI must be due to the characteristic γ-rays of iodine-123 which have energies of 159 keV. The range of the Auger electrons from iodine-123 would be <10 nm (Howell, 1992). This is insufficient to reach the cell nucleus from the extracellular region. 4-[^{123}I]Iodoantipyrine can enter the cells because the organic antipyrine molecule is lipid and membrane compatible. This facilitates entry into the nucleus and result in interaction of the Auger electrons with the DNA target. The micronuclei results are consistent with the notion that iodine-123 has entered the nucleus and causes a higher radiotoxicity than [^{123}I]NaI. The latter does not reach the DNA target, and hence causes a low MN frequency (Fig. 3.8-3.10).

For a given cell biological endpoint it can be expected for radiosensitive and radioresistant cells to be inactivated by Auger electrons (^{123}I) with near equal effectiveness. This follows from cell inactivation by high-LET irradiation (Hall 1988, Slabbert *et al*, 1996). When such an experiment was conducted with 4-[^{123}I]iodoantipyrine, which conceivably disintegrates near the DNA, it was found that cell inactivation by [^{123}I]NaI and long range γ-rays is consistently less effective than cell inactivation by 4-[^{123}I]iodoantipyrine which enters the nucleus (Fig. 3.8-3.10). For high-LET disintegration in the DNA, photon sensitive and photon resistant cells can be expected to respond with similar effectiveness (Hall, 1988), hence the difference between extracytoplasmic irradiation effects and intranuclear

irradiation effects should be higher in radioresistant cells. Table 3.1 and comparison of MN frequencies induced by 4-[^{123}I]iodoantipyrine and [^{123}I]NaI exposure (Fig. 3.11) demonstrates that this is not the case. The results (Fig. 3.11) strongly suggest that the irradiation by 4-[^{123}I]iodoantipyrine in the nucleus is in fact not typical for high-LET radiation. It appears that the 4-[^{123}I]iodoantipyrine does not effectively reach the DNA and sets off indirect radiation effects. The fact that the ratio between the inactivation slopes 4-[^{123}I]iodoantipyrine/[^{123}I]NaI are on average the same (2.3) for a wide variety of cell lines (Fig. 3.11) indeed leaves no other conclusion than that the 4-[^{123}I]iodoantipyrine is in fact not rendering a high-LET irradiation effect. It is possible that antipyrine is in fact trapped by the histone nuclear proteins which compact the DNA and which also contain large hydrophobic domains (Stryer, 1988). Such a protection mechanism is not unrealistic if it is realised that histones and DNA associate in a 1:1 weight ratio and that higher order folding of the nucleosome chain into solenoids, loops, and chromatids generates considerable protein density. In the nucleosome core, the histone octamer measures 7 nm and closely approximates the 10 nm dimension of the Auger electron range. It is suggested that the interlacing of protein density with DNA density suppresses direct ionisation from Auger decay at the DNA and directs the majority of Auger decay to the histones.

When cells are exposed to Auger electrons, one would expect radioprotection by radical scavengers to be ineffective, because high-LET particles are directly ionising (Rao *et al*, 1990). Low-LET γ-rays on the other hand would respond to radical scavengers, because they are indirectly ionising, involving free -OH radicals. The fairly similar dose reduction factors (DRF's) achieved with DMSO to both 4-[^{123}I]iodoantipyrine and [^{123}I]NaI (Table 3.2) demonstrate that both agents operate via the same mechanism i.e. indirectly. This conclusion is in agreement with recent work by Walicka *et al* (1999) which also suggests an indirect mechanism of radiation damage induced by Auger electrons.

The general conclusions drawn from the 4-[^{123}I]iodoantipyrine/[^{123}I]NaI experiments are that the two iodine-123 carriers differ in radiobiological effectiveness, with the 4-[^{123}I]iodoantipyrine emerging as the more radiotoxic compound. The higher radiotoxicity of the 4-[^{123}I]iodoantipyrine can be attributed to the fact that this compound enters the nucleus (Kassis *et al*, 1999). Cell inactivation by 4-[^{123}I]iodoantipyrine nevertheless emerges to be low-LET in character and this contradicts current thinking about the relationship between the range of Auger electrons and the dimensions of DNA. The discrepancy can be resolved by observing the structural relationship between DNA and histone oligomers which form a fundamental particle (nucleosome) in which the DNA is folded around a histone octomer. The protection of DNA by histones would be particularly pronounced at higher order structure i.e. the 32 nm solenoids, the 200 nm folded loops or 700 nm chromatids (Stryer 1988, Mathews and Van Holde 1990), where the nucleosome chain is tightly folded. A crossection of such higher order chromatin folds shows sandwich structure with low DNA density alternating with high protein density, as drawn (fig. 3.15). In such a structure the chances of Auger decay occurring at the histone protein is considerably higher than at the DNA (fig. 3.16). This could explain the indirect ionization observed.

Auger electron decay from iodine-125 has been modelled and it was concluded that the DNA is not necessarily destroyed by direct hits (Pomplun, 1991). Monte Carlo simulation of electron track structure of localised iodine-125 decay in DNA now incorporate aspects of native chromatin structure showing a heterogeneous target. (Pomplun *et al* 1996, Pomplun and Terrissol 1994).

REFERENCES

Akudugu J. M., J.P. Slabbert, A. Serafin and L. Böhm, Radiation-induced micronuclei frequency in neuronal cells does not correlate with clonogenic survival. *Rad. Res.* (in press).

Almassy Z., B. Krepinsky, A. Bianco and G. J. Koteles, The present state and perspectives of micronucleus assay in radiation protection. A review. *Appl. Radiat. Isot.* **38**, 241-249 (1987).

Capala J., M. Makar and J. Coderre, Accumulation of boron in malignant and normal cells incubated *in vitro* with boronophenylalanine, mercaptoborane or boric acid. *Radiat. Res.* **146**, 544-560 (1996).

Emslie-Smith D. (ed), Textbook of Physiology, Chapter 2. New York, Churchill Livingstone, (1988).

Freshney R. I., Culture of animal cells: A manual of basic technique, New York, Alan R. Liss, Inc., (1983).

Guo G. Z., K. Sasai, N. Oya, T. Takagi, K. Shibuya and M. Hiraoka, Simultaneous evaluation of radiation-induced apoptosis and micronuclei in five cell lines. *Int. J. Radiat. Biol.* **73**, 297-302 (1998).

Hall E. J., Radiobiology for the Radiologist. Philadelphia, Lippincott Company, (1988).

Hofer K. G., Symposium report: Biophysical aspects of Auger processes. *Int. J. Radiat. Biol.* **61**, 289-292 (1992).

Hofer K. G. and S. Bao, Low-LET and high-LET radiation action of ^{125}I decays in DNA: Effect of cysteamine on micronucleus formation and cell killing. *Radiat. Res.* **141**, 183-192 (1995).

Howell R. W., Radiation spectra for Auger-electron emitting radionuclides: Report No. 2 of AAPM Nuclear Medicine Task Group No. 6. *Med. Phys.* **19**, 1371-1383 (1992).

Humm J. L., R. W. Howell and D. V. Rao, Dosimetry of Auger-electron-emitting radionuclides: Report No. 3 of AAPM Nuclear Medicine Task Group No. 6. *Med. Phys.* **21**, 1901-1915 (1994).

Johns H. E., The physics of radiology. Springfield, Charles C. Thomas, (1974).

Kassis A. I., Toxicity and therapeutic effects of low energy electrons. *Nucl. Ins. Met. Phys. Res.* **27**, 279-284.

Kassis A. I. and S. J. Adelstein, A Rapid and Reproducible Method for the Separation of Cells from Radioactive Media. *J. Nucl. Med.* **21**, 88-90 (1980).

Kassis A. I., R. Harapanhalli and J. Adelstein, Comparison of Strand Breaks in Plasmid DNA after Positional Changes of Auger Electron-Emitting Iodine-125. *Radiat. Res.* **151**, 167-176 (1999).

Kearney T., A. Hughes, R. Hanson and E. DeSombre, Radiotoxicity of Auger Electron-Emitting Estrogens in MCF-7 Spheroids: A Potential Treatment for Estrogen Receptor-Positive Tumors. *Radiat. Res.* **151**, 570-579 (1999).

Keele C. A., E. Niel and N. Jones, Samson Wright's applied physiology, Part 1. Oxford, Oxford University Press, (1982).

Ludwikow G., F. Ludwikow and K. J. Johanson, Kinetics of micronucleus induction by ^{125}I-labelled thyroid hormone-responsive cells. *Int. J. Radiat. Biol.* **61**, 639-653 (1992).

Mathews C. and K. E. Van Holde, Biochemistry. Redwood City, Benjamin-Cummings, (1990).

Miyazaki N. and K. Shinohara, Cell Killing Induced by Decay of ^{125}I during the Cell Cycle: Comparison of ^{125}I-Antipyrine with ^{125}I-Bovine Serum Albumin. *Radiat. Res.* **133**, 182-186 (1993).

Ono K., S. Masunaga, M. Akaboshi and K. Akuta, Estimation of the initial slope of the cell survival curve after irradiation from micronucleus frequency in cytokinesis-blocked cells. *Radiat. Res.* **138**, S101-S104 (1994).

Persson L., The Auger electron effect in radiation dosimetry. *Health Physics* **67**, 471-476 (1994).

Pomplun E., A new DNA target model for track structure calculations and its first application to I-125 Auger electrons. *Int. J. Radiat. Biol.* **59**, 625-642 (1991).

Pomplun E., M. Terrissol, Low-energy electrons inside active DNA models: a tool to eludicate the radiation action mechanisms. *Radiat. Environ Biophys.* **33**, 279-292 (1994).

Pomplun E., M. Terrissol, M. Demonchy, Modelling of initial events and chemical behaviour of species induced in DNA units by Auger electrons from ^{125}I, ^{123}I and carbon. *Acta Oncologica* **35**, 857-862 (1996).

Rao D., V. Narra, R. Howell and K. Sastry, Biological consequence of nuclear versus cytoplasmic decays of ^{125}I: Cysteamine as a radioprotector against Auger cascades *in vivo*. *Radiat. Res.* **124**, 188-193 (1990).

Slabbert J. P., J. H. Langenhoven, B. S. Smit, Synthesis of [^{123}I]iodoantipyrine to study the high-LET characteristics of Auger electrons in mammalian cells. *J. Radioanalytical Nucl. Chem*. **240**, 505-508 (1999).

Slabbert J. P., T. Theron, A. Serafin, D. T. L. Jones, L. Bohm and G. Schmitt, Radiosensitivity variations in human tumor cell lines exposed *in vitro* to p(66)/Be neutrons or ^{60}Co γ-rays. *Stralenther. Onkol.* **172**, 567-572 (1996).

Stryer L., Biochemistry 3rd ed, New York, W.H. Freeman Co., (1988).

Walicka M., G. Vaidyanathan, M. Zalutsky, J. Adelstein and A. Kassis, Survival and DNA damage in Chinese hamster V79 cells exposed to alpha particles emitted by DNA-incorporated Astatine-211. *Radiat. Res.* **150**, 263-268 (1998).

Walicka M., Y. Ding, J. Adelstein and A. Kassis, Dimethyl sulfoxide decreases double-strand break induction and toxicity from decay of ^{123}I in DNA of frozen mammalian cells. *Radiat. Res. Vol. 1. Congress Abstrascts*, 111 (1999).

APPENDIX

1. Aspects of radiation action

Radiobiology is the study of the effects of ionizing radiation on living matter. The absorbed radiation transfers energy to orbital electrons that are ejected. This results in ionization and breakage of chemical bonds and release of energy. Each ionizing event releases approximately 33 eV, whereas 4.9 eV is needed to break a -C-C- bond. The destruction of DNA causes lethal events and the cell dies.

a. Electromagnetic radiation

In the electromagnetic spectrum X- and γ-rays have high photon energies, high frequencies and short wavelengths, compared to the low energies, low frequencies and long wavelengths of radio waves at the other end of the spectrum. Electromagnetic radiation is regarded as ionizing when its photon energy is larger than 124 eV, which corresponds to a wavelength of less than 10^{-6} cm. X- and γ-rays posses enough energy to cause ionization and are therefore useful for medical applications and radiobiological experiments. The nature and properties of X- and γ-rays are very similar, but they differ in the way they are produced. X-rays are produced extranuclearly in a 'cathode ray tube' and γ-rays intranuclearly by decay of radioactive isotopes, e.g. ^{60}Co . The Gray (Gy) is the unit of absorbed dose and it corresponds to energy absorption of 1 joule/kg. The mean lethal whole body dose for humans is about 4 Gray. However, this will only cause a temperature rise of 0.002 °C in the body.

b. Particulate radiation

Particulate radiation consists of atomic fragments. These particles can be uncharged like neutrons or can carry an electrical charge as in the case of electrons, protons, alpha particles or other ions.

Neutrons have the same mass as protons, but posses no electrical charge. They can therefore not be accelerated, but are produced as a by-product of fission in, for example, nuclear reactors. Neutrons are also produced when a charged particle, like a proton, is accelerated to high energy and directed onto an appropriate target like beryllium. This results in nuclear reactions causing neutron emission. The penetration depth of neutrons in tissue depends on their energy.

Electrons are very small negatively charged particles and can be accelerated to close to the speed of light. At these high energies they can pass right through the human body. Electrons are also emitted during the decay of radioactive nuclei. Electrons emitted in such a way are referred to as beta-rays and can be of two types: Beta (-), electrons or Beta (+), positrons. The penetration depth of β-rays is typically 5 mm in tissue.

Protons are positively charged particles and are almost 2000 times heavier than electrons. A proton is a hydrogen nucleus and can be accelerated to useful energies using a cyclotron. At the NAC protons are accelerated to 200 MeV with a resulting penetration depth of 26.3 cm in human tissue.

Alpha particles consist of two protons and two neutrons and are the nuclei of helium atoms. Alpha particles have a net positive charge and can be accelerated in the same way as protons. Alpha particles are also emitted during the radioactive decay of many heavy nuclei e.g. radium and uranium. These alpha particles have a range in tissue of ± 0.04 mm.

Heavy ions of elements like carbon or neon are positively charged, by stripping some of the orbital electrons. Heavy ions can be accelerated at only a very limited number of laboratories in the world. They are also by-products of the fission process at nuclear power plants or atom bombs and they have high-LET properties.

2. Isotopes

Isotopes contain the same number of protons in the nucleus and have the same extra-nuclear electronic structure as the parent element, but differ in the number of neutrons. Isotopes of a specific element cannot be distinguished chemically and undergo the same chemical reactions.

$^{1}_{5}{}^{2}_{3}{}^{3}$I indicates an isotope of iodine (atomic number 53) with a total of 123 nucleons (protons + neutrons). The atomic number is synonymous with the chemical symbol and the isotope is therefore usually just written as ^{123}I.

Most isotopes are unstable and emit radiation. These are called radioactive isotopes, radioisotopes or radionuclides. Some isotopes are stable and do not spontaneously emit radiation. Some radioactive elements, such as radium, are found in nature, but most other radioactive materials are artificially produced in nuclear reactors or by accelerators. An accelerator is a device that accelerates charged particles to high velocities. A nuclear reactor can produce many different types of isotopes simultaneously, whereby an accelerator can often only produce a limited number of isotope at a time. Radioactive isotopes are widely used in diagnostic and therapeutic nuclear medicine.

a. Medical uses

a.1. Diagnostic:

Radiopharmaceuticals play an essential part in the diagnostic procedure during many clinical investigations. Gamma cameras, detecting the emitted gamma rays, are used to construct computer images of the spatial distribution of the radionuclide in the organ as well as the dynamics of the processes. Better imaging techniques and better radiopharmaceuticals would provide more diagnostic information for smaller quantities of administered radioactivity. The trend is also to use gamma emitters which emit few or no β-particles and to use radionuclides with a shorter

half live. The use of iodine-123 has largely replaced the longer-lived iodine-131 in diagnostic tests. Iodine-123 is readily available at NAC for radiobiological studies.

a.2. Therapeutic:

A medical condition where radionuclides are commonly applied, is the treatment of hyperthyroidism with iodine-131. Iodine naturally concentrates in the thyroid gland and a big enough dose can therefore be delivered selectively to kill cells and suppress proliferation.

In radioimmunotherapy (RIT) the radionuclide is labelled to monoclonal antibodies that target a specific cell type. RIT is already capable of treating B-cell-lymphomas, chronic lymphocytic leukemia and breast- and prostate cancer. Various clinical trials are in progress to expand the use of RIT for cancer treatment. The damaging properties of short range particles like Auger electrons or alpha particles, emitted by some radionuclides, are being investigated by radiobiologists. The alpha emitter astatine-211, shows great potential as a radiotherapeutic agent (Walicka *et al*, 1998).

b. Isotope manufacturing

Radionuclides used in Nuclear Medicine fall into two categories i.e. reactor and accelerator produced:

b.1. Role of reactors.

Thermal neutrons from a nuclear reactor can be used to manufacture isotopes. In this process a neutron is added to the element, without a change in the number of protons. The same element is therefore still present in the product and the reaction is written as (n, gamma), indicating the addition of a neutron with the subsequent emission of a gamma ray. During the fission process of uranium-235 in a nuclear reactor, certain isotopes are also produced as a by-product, which can be suitable for medical use. Molybdenum-99, xenon-133 and iodine-131 are such isotopes that

result from the fragmentation of the unstable uranium-236, formed when a neutron is added to uranium-235 in the reactor.

b.2. Role of cyclotrons.

Cyclotrons accelerate protons, deuterons or other charged particles to high energies. A beam of the accelerated particles is directed onto an appropriate target to produce the required isotope. Nuclear reactions take place according to the nature of the beam and the target e.g. (d, n), (p, pn), (p, 5n), (p,α), The net effect is a change in A-number and/or Z-number of the target nucleus (increase in neutrons or protons or both). In most cases a different element is formed and chemical separation techniques are used to separate the required isotope from the rest of the target.

c. Production of iodine-123

At the National Accelerator Centre 66 MeV protons are used to bombard a sodium-iodide target to produce iodine-123. When a proton hits iodine-127, five neutrons are dislodged, resulting in xenon-123, which immediately disintegrates to iodine-123.

d. Synthesis of 4-Iodoantipyrine

The following text is a summary of the method described by Slabbert *et al* (1999) for the synthesis of 4-[^{123}I]Iodoantipyrine.

Antipyrine ($C_{11}H_{12}N_2O$) is a white crystalline powder soluble in water, alcohol, chloroform and ether. It is soluble in polar and non-polar liquids and hence diffuse through the cellular membranes. These properties facilitate entry of 4-[^{123}I]iodoantipyrine into the cells. 4-[^{123}I]Iodoantipyrine is not commercially available, hence labeling of the antipyrine molecule with iodine-123 must be accomplished. The labeling method must produce a product that complies with two important requirements namely, absence of reagents that could have an adverse effect on cells in culture and a high enough specific activity to render the antipyrine effective

as a carrier. The labeling method used was NaI + antipyrine + chloramine-T (oxidant) → 4-iodoantipyrine. Sodium dihydrogen phosphate (NaH_2PO_4) was used to adjust the pH of the reaction solution to facilitate isotope exchange to accomplish replacement of iodine-127 by iodine-123. Sodium dihydrogen phosphate is biologically acceptable and need not be removed after the synthesis. Final purification of the product by ion exchange yields 4-[^{123}I]iodoantipyrine, with a purity consistently > 98% as analyzed by HPLC.

2. Radiation effects on biological systems

a. Direct and indirect action of radiation

The DNA molecule is the critical target of radiation. Interaction of radiation with orbital electrons results in ionization of DNA components. This is described as direct action of radiation. Since cells consist mostly of water another important reaction is the generation of OH^- (free radicals) and the indirect action upon the DNA molecule. It is estimated that free radicals produced within 1 nm from the DNA double helix (2 nm in diameter) will give rise to interaction and generate DNA damage. (Fig. 1) The ionization of water can be expressed as:

$$H_2O \rightarrow H_2O^+ + e^-$$

The H_2O^+ ion possesses an unpaired electron in the outer shell, which makes it highly reactive. It is therefore called an ion radical. It has an extremely short lifetime of approximately 10^{-10} seconds and decays to form free radicals:

$$H_2O^+ + H_2O \rightarrow H_3O^+ + OH^-$$

The hydroxyl radical is highly reactive and diffuses to the critical target of the cell. Free radicals interfere with the chemical bonds of the DNA molecule. Single or double strand breaks may result. Single strand breaks are readily repaired by the cell and are usually of little consequence. DNA double strand breaks disrupt both strands of the double helix. This could result in lethal lesions, mutations and ultimately in carcinogenesis.

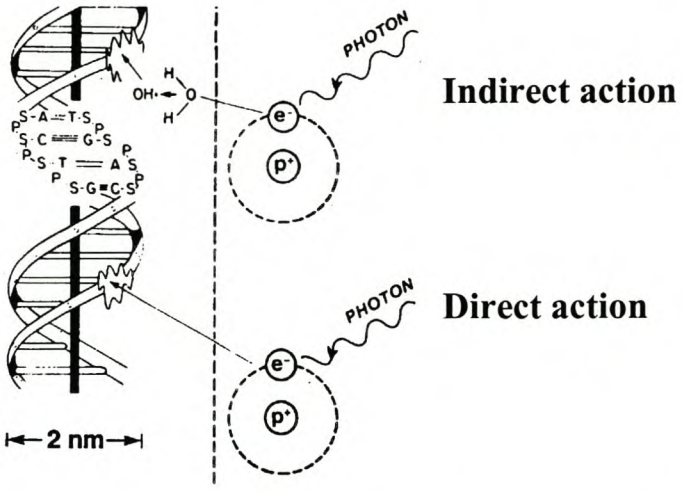

Fig. 1. Illustration of the direct and indirect action of radiation (Hall, 1988).

b. Detection of DNA damage

Double strand breaks produce DNA fragments. These fragments can behave in a variety of ways:

1. The fragments may rejoin in their original configuration and result in normal mitosis.
2. When the fragments fail to rejoin abberations may be formed because of base deletions.
3. Fragments may rejoin incorrectly not obeying the original DNA sequence and give rise to misrepaired chromosomes.

Fluorescent in situ hybridization (FISH) techniques can identify DNA abberations and correlate them with the irradiation delivered. Some abberations are lethal, like the dicentric, ring and anaphase-bridge. Others may be non-lethal like translocations and deletions.

Micronuclei formed during division of nuclei (karyogenesis) in mitosis represent DNA damage and micronuclei can be scored by fluorescent microscopy. Micronuclei arise either from acentric fragments that fail to be incorporated into the daughter nuclei

during mitosis or from whole chromosomes that lag behind in anaphase due to centromeric dysfunction, a defective spindle apparatus or complex chromosomal rearrangements. There is a direct relationship between the micronuclei frequency observed and the amount of radiation damage caused to the cells.

The clonogenic assay of cell survival provides means to evaluate reproductive integrity of cells. When a cell survives a radiation injury and retains its reproductive integrity it is scored as a colony, usually representing 10-20 mitotic divisions. Clonogenic assays are the gold standard of radiobiological analysis as they represent comprehensive evidence of the proportion of cells that have retained reproductive integrity. (Fig. 2).

2 Gy **0 Gy (Control)**

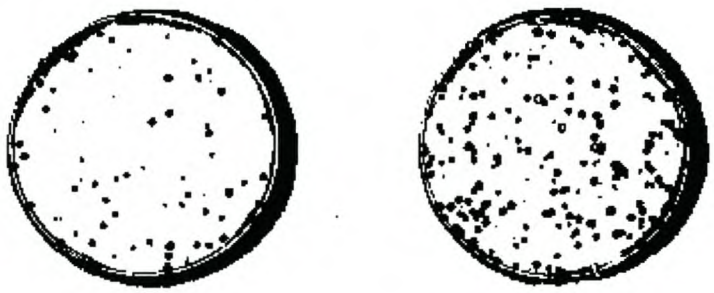

Fig. 2. Colonies of CHO-K1 cells as grown in 60 mm petri dishes.

4. Cancer therapy

In industrial societies about one in three people will get cancer, but only one in five will die of it. Radiotherapy and surgery are still the most effective methods used for curing cancer patients. About half of all cancer patients receive radiotherapy at some stage of their disease and the development of new radiation treatment strategies is continuing.

Photon irradiation, using X- or gamma rays, is most generally used to treat tumors. The fast dividing cells of most tumors are more radiosensitive than normal tissue. The rationale behind radiotherapy is therefore that the tumor cells will be harmed

more than the normal cells when a dose is given to a deep-seated fast-growing tumor. The high penetration depth, low skin dose and relatively cheap production cost makes photon irradiation the most popular radiation modality used today. Similar advantages apply for electrons from linear accelerators used for therapy.

Hypoxic regions in some tumors cause photon and electron therapy to be unsuitable because of the absence of the radiosensitizing effects of oxygen in the hypoxic regions of these tumors. The oxygen enhancement ratio (OER) for X- and gamma rays is in the region of 2.5 - 3 *in vitro* (Hall, 1988). High-LET radiation has a lower OER and is therefore more suitable for the treatment of hypoxic tumors. Fast neutrons are uncharged heavy particles that produce charged heavy particles, mostly protons, when entering tissue. These particle tracks are densely ionizing and a neutron beam is therefore high-LET radiation. Neutrons are a lot more expensive to produce than X- or gamma rays, but are cheaper to produce than charged heavy particles like protons, which require large accelerators.

The phenomenon of the Bragg peak, where the dose deposited by protons increases slowly to a maximum near the end of the particle's range, makes protons attractive for radiotherapy. It is possible to focus the high dose region in the tumor volume, with minimal dose to the surrounding normal tissue. It is expensive to produce a proton beam with a high enough penetration depth to be useful for therapy. (At NAC a 200 MeV proton beam with a penetration depth of 26,3 cm in tissue is produced.)

Boron neutron capture therapy requires cells to be loaded with ^{10}B and irradiated with slow neutrons. The direct effect of slow neutrons in tissue is slight and the ^{10}B atoms capture the neutrons with the consequent emission of an alpha particle and ^{7}Li recoils and some gamma rays. The particle ranges are less than the diameter of a cell and cause extremely localized high-LET damage. Boron neutron capture therapy aims to enhance the dose to the tumor to the maximum with the minimum of external dose deposited in normal tissue.

Radioimmunotherapy eliminates the need for an external beam completely by delivery of a radionuclide to the cells in the tumor volume itself. Various radionuclides have been considered for cancer therapy, including alpha particle emitters and Auger electron emitters. Auger electrons are potentially suitable for cancer therapy, because their radiobiologic effectiveness is even higher than that of high-LET α-particles. If suitable methods for selective radionuclide delivery to cancer cells can be developed, Auger electron emitters could one day provide a means of realizing Paul Ehrlich's dream of a 'magic bullet' in cancer therapy. (Hofer, 1992)